Communications Research Centre Canada
An Agency of Industry Canada

Centre de recherches sur les communications Canada
Un organisme d'Industrie Canada

Evaluation of RF Exposure from an FM (88-108MHz) Radio Broadcasting Antenna (Phase II Study)

M. Zhang and A. Alden

REMC/VPTWS

Ottawa, October 2010

CRC Report No. 2010-003

Canada

Communications Research Centre Canada
An Agency of Industry Canada

Centre de recherches sur les communications Canada
Un organisme d'Industrie Canada

Evaluation of RF Exposure from an FM (88-108MHz) Radio Broadcasting Antenna (Phase II Study)

M. Zhang and A. Alden

REMC/VPTWS

Ottawa, October 2010

CRC Report No. 2010-003

Canada

List of Tables

List of Figures

1. Introduction

This study continues an investigation into the interaction of RF waves with a human body. In Phase I of this study [1], a direct relationship was established between RF maximum power density and the specific absorption rate (SAR) caused by mobile base station antennas (800 and 1900 MHz cellular/PCS). Empirical formulas were developed to predict the variation of SAR values with distance, frequency and antenna pattern. Compliance analyses regarding the SAR limit and compliance distance, were carried out using these formulas.

The present report covers Phase II of the project. It is specific to SAR calculations at a typical FM broadcasting frequency of 100 MHz.

1.1 Background

Human exposure is usually quantified in terms of the specific absorption rate (SAR), which is the time derivative of dissipated energy per unit mass within the exposed body, caused by an incident electromagnetic field. Specifically, SAR is defined as the power absorbed per unit mass of tissue, usually being averaged either over the whole body, or over a small sample volume (typically 1g or 10g of tissue). Safety guidelines for limiting electromagnetic field exposure have been published by the International Commission on Non-Ionizing Radiation Protection (ICNIRP) [2], Health Canada [3], and the Institute of Electrical and Electronics Engineers (IEEE) [4]. In most countries these guidelines have been adopted as the basic restrictions on SAR, to prevent adverse health effects related to whole-body heat stress and excessive localized tissue heating, for frequencies between 100 kHz and 300 GHz.

Accurate RF dosimetry measurements in simulated full human bodies are complex. They require fabricated phantom models with various tissue geometries and specially developed liquids for tissue-equivalent materials, and a robot fitted with a measurement probe [5, 6]. Various numerical simulation techniques are now available and provide effective alternative methods to determine SAR distributions in highly sophisticated millimeter-resolution anatomically based models. Among those techniques, the finite-difference time-domain (FDTD) method has become the most widely used method for bio-electromagnetic applications.

1.2 Objective

The purpose of this project is to establish a direct relationship between maximum RF transmitted power and the specific absorption rate (SAR) when a human body is exposed to RF emission from an FM broadcasting antenna.

In order to investigate the direct relationship between the maximum transmitted power and the SAR, a worst-case scenario has been considered, in which the incoming radio signal is in a line-of-sight path to a human body on a soil ground with no surrounding structures, trees etc. Calculations have been performed as the body model was moved up to 60 metres away from the antenna. At each location, whole-body average and peak spatial-averaged SAR values over 1- and 10- g mass were evaluated in accordance with IEEE Standard C95.3-2002 (R2008) [7].

The report is organized as follows:

Chapter 2 gives brief descriptions of the anatomical full-body models, the FM broadcasting antenna, the electromagnetic simulation tool, and the computer simulation setup used in this study.

Simulation results are presented in Chapter 3. Whole-body average and peak spatial-averaged SAR values over 1- and 10- g mass are calculated as the body is moved away from the antenna. Locations of tissues with peak spatial-averaged SAR values are determined.

In Chapter 4, based on the numerical study, an empirical formula is developed to describe the variation of SAR values with horizontal distance. With the formula, compliance analysis regarding the SAR limit with respect to distance can be carried out.

Chapter 5 summarizes the results and proposes further work.

2. Numerical Models and Computer Modeling

2.1 Introduction

This chapter presents details of the anatomically based full-body models, the electromagnetic simulation tool, and the 100 MHz broadcasting antenna. A powerful calculating engine based on the Finite Difference Time Domain (FDTD) method from Empire [8] will be used in this study.

2.2 Anatomical Full-Body Models and Numerical Solver

Table 2.1 summarizes the four full-body anatomical models used in this study. The first two models are Magnetic Resonance Imaging (MRI)-based models (Figure 2.1) with 84 different tissues and organs, and the other two body-like (BL) models use 40 different tissues (Figure 2.2). The MRI models were obtained from the ITIS Foundation [9], and the BL models from Empire. **Note that model dimensions were determined using individuals in a supine position.** When rotated to the vertical, body length from the ground is larger than true height because the lying-down position of the feet during dimensional measurements translates to a tip-toe position in the vertical.

Table 2.1 The Four Body Models

Models	Magnetic Resonance Imaging (MRI)		Body-Like Model (BL)	
Names	Duke	Billie	N/A	N/A
Age and Gender	34 year-old male	11 year-old girl	Male Adult	10 year-old boy
Weight (kg)	71.5	35.0	71.68	32.5
Height (m)	1.81	1.46	1.86	1.38

In Empire, the frequency dependence of the electromagnetic parameters of the tissues is calculated using the Debye model. The human tissues have high relative permittivity values (ε_r), mostly ranging from 30 to 90. The conductivity values (σ) of the tissues are high enough that

the human body is quite "lossy" or absorbent of energy. Tables 2.2 and 2.3 give the parameters for the tissues at 100 MHz for both models. Excellent agreement is obtained when comparing these calculated parameters with values from the Italian National Research Council [10] and FCC web pages [11].

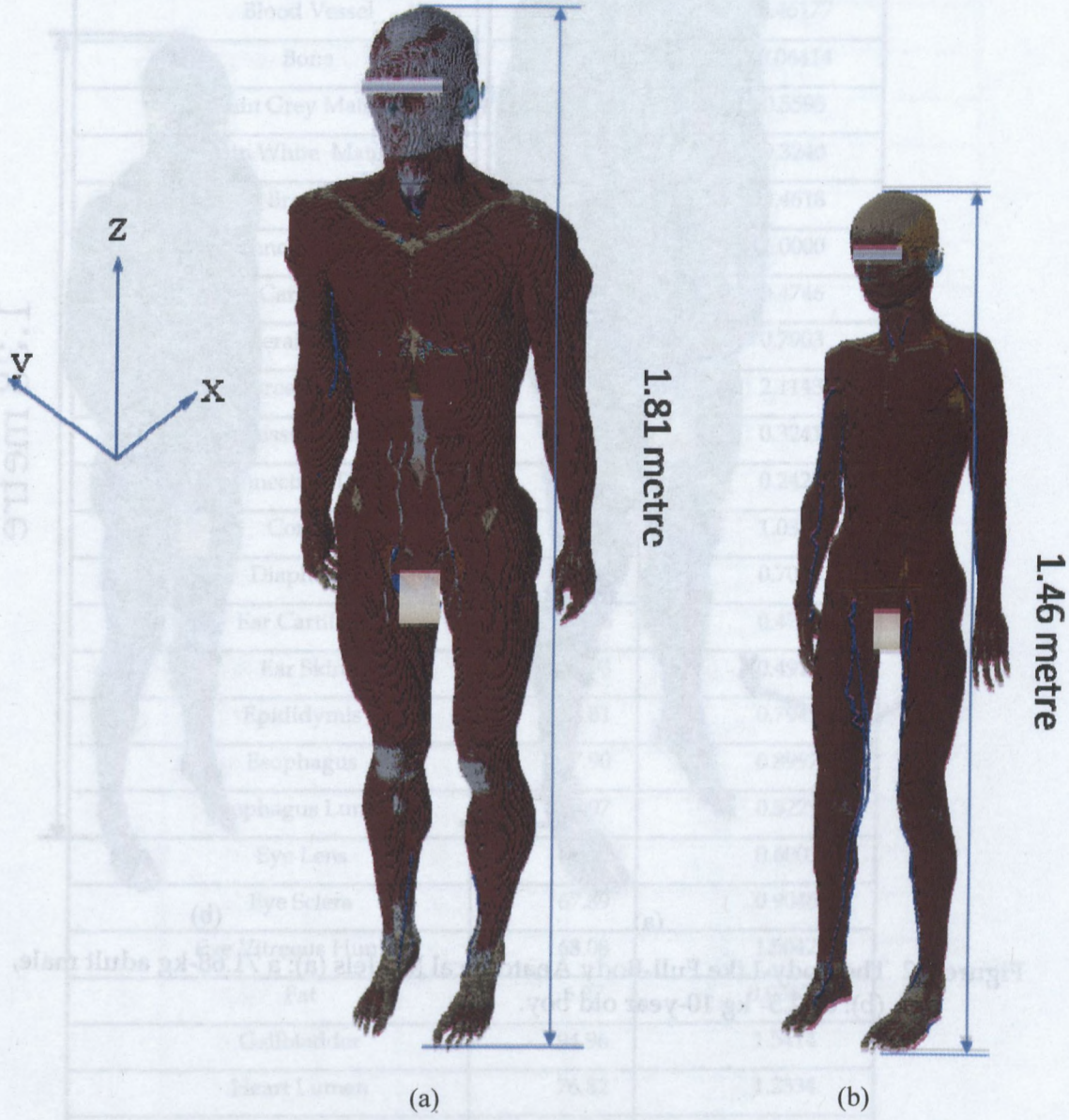

Figure 2.1 The MRI Full-Body Anatomical Models (a): a 71.5-kg adult male (Duke), (b): a 34.8-kg 11-year old girl (Billie).

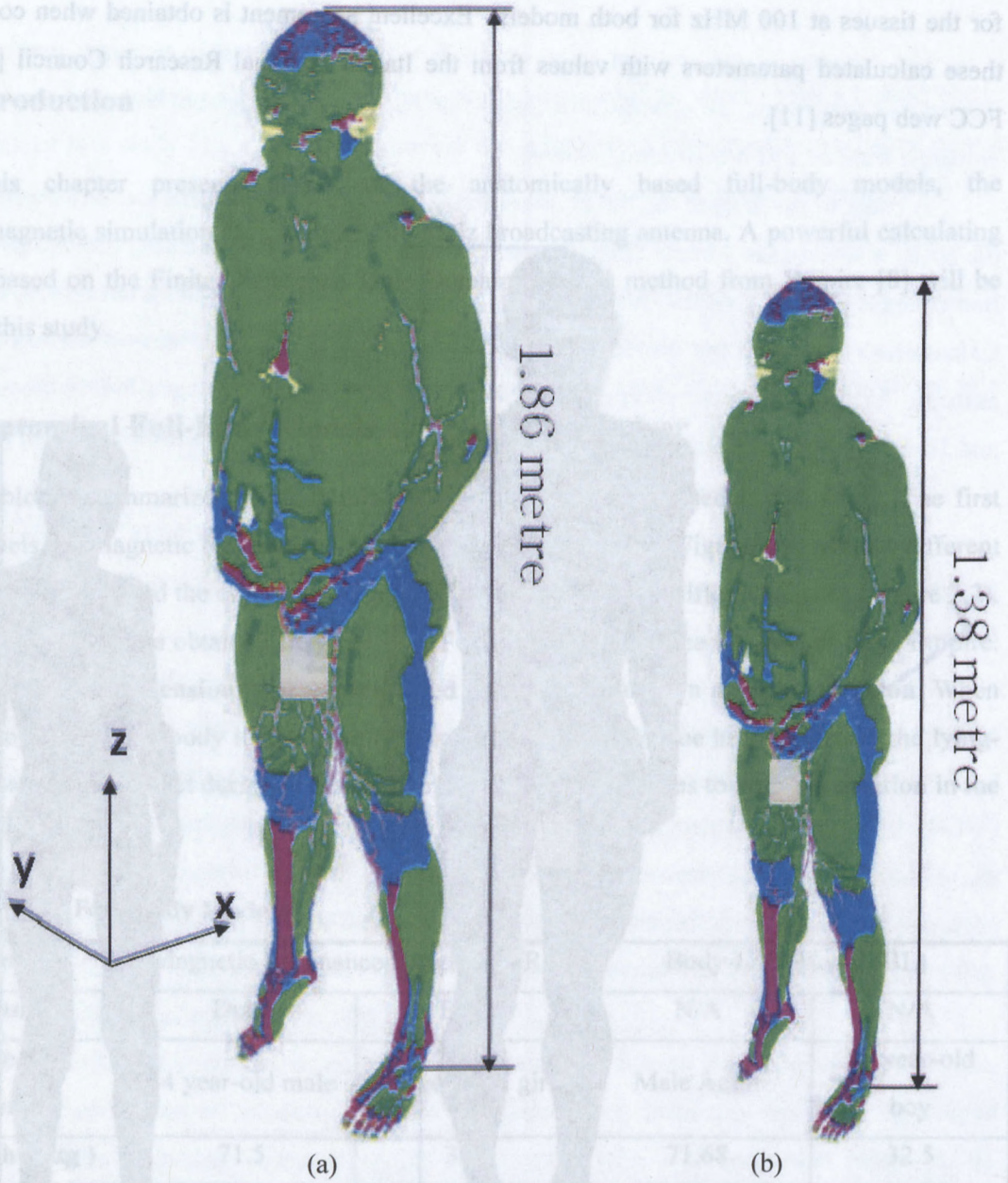

Figure 2.2 The Body-Like Full-Body Anatomical Models (a): a 71.68-kg adult male, (b): a 32.5- kg 10-year old boy.

Table 2.2 Dielectric Constant ε_r and Conductivity σ of Tissue of MRI Anatomical Models at 100 MHz

Tissues	ε_r	σ (mS)
Adrenal Gland	68.81	0.7943
Artery	76.82	1.2330
Bladder	22.65	0.29394
Blood Vessel	59.78	0.46177
Bone	15.28	0.06414
Brain Grey Material	80.14	0.5595
Brain White Material	56.80	0.3240
Bronchi	59.78	0.4618
Bronchi Lumen	1.0	1.0000
Cartilage	55.76	0.4746
Cerabellum	89.77	0.7903
Cerebrospinal Fluid	89.90	2.1143
Commissura Anterior	56.80	0.3241
Connective Tissue	28.70	0.2423
Cornea	76.04	1.0368
Diaphrage	65.97	0.7076
Ear Cartilage	55.76	0.4746
Ear Skin	72.93	0.4910
Epididymis	68.81	0.7943
Esophagus	77.90	0.8997
Esophagus Lumen	65.97	0.5229
Eye Lens	55.10	0.6003
Eye Sclera	67.89	0.9046
Eye Vitreous Humor	68.08	1.5042
Fat	6.07	0.03629
Gallbladder	94.96	1.5414
Heart Lumen	76.82	1.2334
Heart Muscle	90.82	0.7330

Table 2:2 Cont'd.

Hippocampus	80.14	0.5946
Hypophysis	68.81	0.7943
Hypothalamus	68.81	0.7943
Intervertebral Disc	55.76	0.7476
Kidney Cortex	98.09	0.8106
Kidney Medulla	98.09	0.8106
Large Intestine	81.80	0.6801
Large Intestine Lum	1.00	0.0000
Larynx	55.76	0.4746
Liver	69.02	0.4872
Lung	31.64	0.3057
Mandible	15.28	0.06431
Marrow Red	14.29	0.1593
Medulla Oblongata	76.46	0.5428
Meniscus	55.76	0.4746
Midbrain	76.46	0.5428
Mucosa	65.97	0.5229
Muscle	65.97	0.7076
Nerve	47.27	0.3381
Pancreas	68.81	0.7943
Patella	15.28	0.6431
Penis	76.82	1.2330
Pharynx	1.00	0.0000
Pinealbody	68.81	0.7943
Pons	76.46	0.5428
Prostate	75.60	0.9109
Sat	6.07	0.03629
Skin	72.93	0.4910
Skull	15.28	0.06431
Small Intestine	96.55	1.6555

Table 2:2 Cont'd.

Small Intestine Lum	1.00	0.0000
Spinal Cord	47.27	0.3381
Spleen	90.66	0.8015
Stomach	77.90	0.8997
Stomach Lumen	1.00	0.0000
Teeth	15.28	0.06431
Tendon Ligament	53.92	0.4902
Testis	75.60	0.9109
Thalamus	80.14	0.5595
Thymus	68.81	0.7943
Thyroid Gland	68.81	0.7943
Tongue	67.89	0.6740
Trachea	55.76	0.4786
Trachea Lum	1.00	0.0000
Ureter Urethra	59.78	0.4618
Vein	76.82	1.2330
Vertebrae	15.28	0.06430

Table 2.3 Dielectric Constant ε_r and Conductivity σ of Tissue of Body-Like Anatomical Models at 100 MHz

Tissues	ε_r	σ (mS)
Bile	94.97	1.5414
Body Fluid	69.08	1.5042
Eye Cornea	76.04	1.0369
Fat	6.07	0.03629
Lymph	68.81	0.7943
Mucous Membrane	65.97	0.5233
Nails (Toe & Finger)	15.28	0.06431
Nerve (Spine)	47.27	0.3382
Muscle	65.97	0.7076
Heart	90.82	0.73301
White Material	56.80	0.32405
Stomach	77.90	0.8997
Glands	68.81	0.7943
Blood Vessel	59.78	0.4618
Liver	69.02	0.4872
Gall Bladder	79.00	1.0137
Spleen	90.66	0.8016
Cerebellum	89.77	0.7903
Bone (Cortical)	15.28	0.0643
Cartilage	55.76	0.4746
Ligaments	53.92	0.4902
Skin/Dermis	72.93	0.4812
Intestine (Large)	81.80	0.6801
Tooth	15.28	0.06431
Gray Material	80.14	0.5595
Eye (Lens)	55.10	0.6003
Lung (Outer)	67.11	0.5588

Table 2:3 Cont'd.

Intestine (Small)	96.55	1.6555
Eye (Sclera/Wall)	67.89	0.9045
Lung (Inner)	31.64	0.3057
Pancreas	68.81	0.7943
Blood	76.82	1.2330
Cerebral Spinal Fluid	88.91	2.1143
Eye (Aqueous Humor)	69.08	1.5042
Kidney	98.09	0.8106
Bone Marrow	6.49	0.02274
Bladder	22.65	0.2939
Testicles	75.60	0.9109
Bone (Cancellous)	27.63	0.1725

2.3 Antenna and Modeling

A vertical standard half-wave dipole antenna was used as exposure source in this study, as shown in Figure 2.3. Its structure and dimensions are given in Figure 2.4.

Figure 2.3 FM Broadcasting Antenna.

The reflection coefficient of the antenna was calculated and is presented in Figure 2.5. Two blue arrows in this Figure shows the operating range of 90-105 MHz. Figure 2.6 summarizes the radiation characteristics of the antenna, together with the radiation pattern at 100 MHz. In addition, the three-dimensional far-field distribution for the antenna was calculated, and is shown in Figure 2.7. The radiated field distribution of this antenna at 100 MHz is believed to be typical of FM antennas designed for centre frequencies in the range 88-108 MHz.

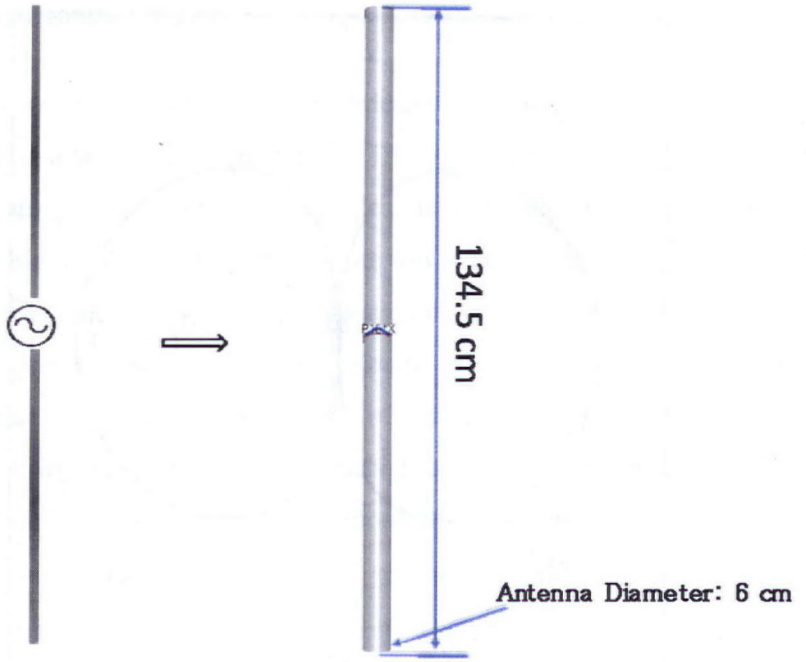

Figure 2.4 100 MHz Half-Wavelength Dipole Antenna: Structure and Dimensions.

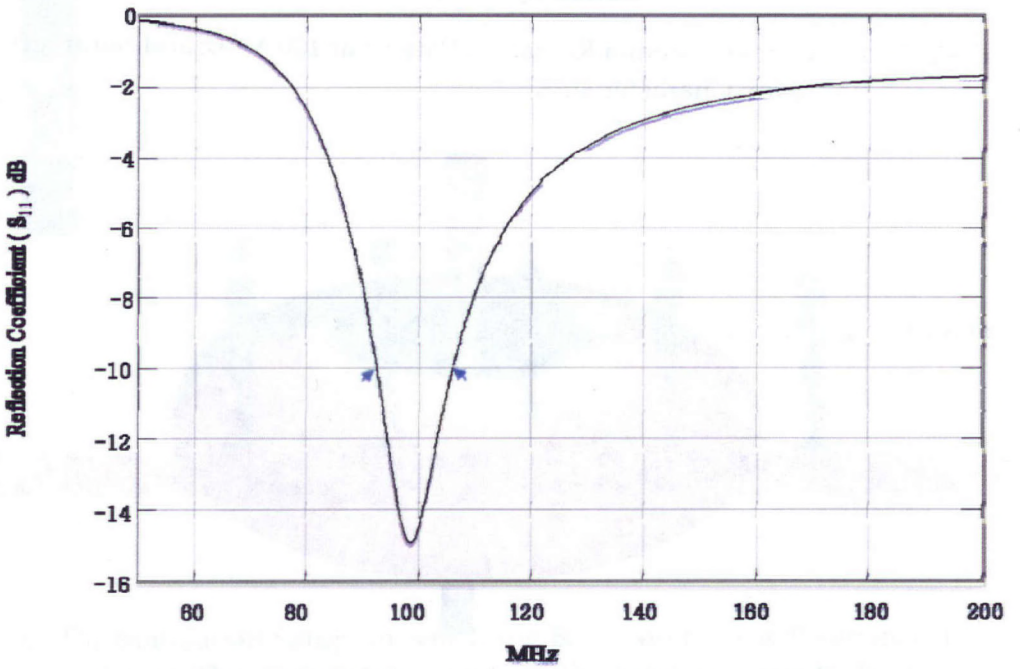

Figure 2.5 100 MHz Half-Wavelength Dipole Antenna: Reflection Coefficient versus Frequency.

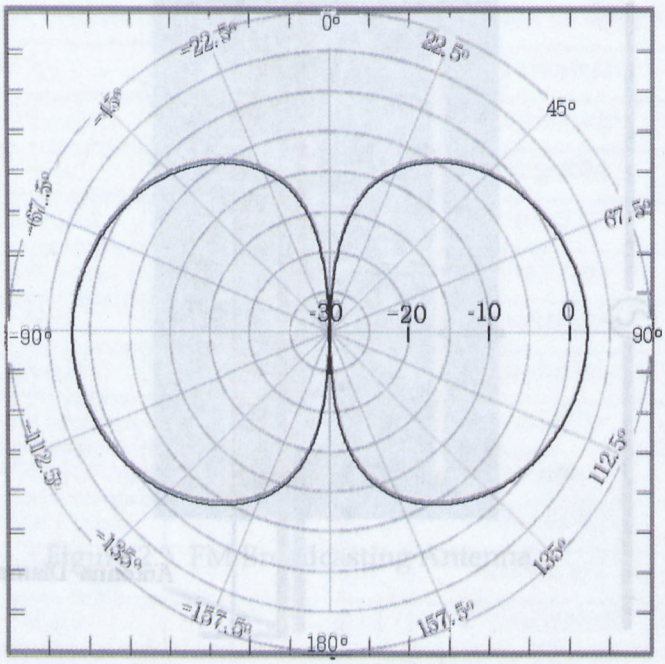

Frequency Range: 90-105 MHz
Half-power beam width: 104°
Directivity: 2.14 dBi

Figure 2.6 FM Dipole Antenna Radiation Pattern at 100 MHz and Summary of Radiation Characteristics.

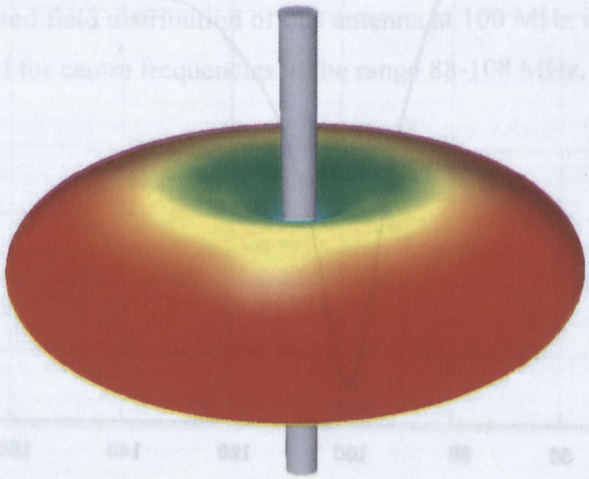

Figure 2.7 100 MHz Half-Wavelength Dipole Antenna: Three-Dimensional Far- Field Distribution.

2.4 Simulation Setup

A common worst-case scenario is considered, in which the incoming radio signal is in a line-of-sight path to a stationary human body. That is, except for a soil ground, described below, surrounding structures, trees etc., are excluded. In the following calculations, the four body models were positioned facing the antenna, the lower end of which was located 15.0 cm above the head. SAR calculations have been performed as the body model was moved up to 60 metres away from the antenna. In our analyses, ground reflection effects have been considered by adding a 45 cm thick good-soil layer (ε_r = 15, σ= 15 mS), which was approximately 13.0 metres wide and bounded by multiple perfectly matched layer (PML) boundary conditions. Figure 2.8 illustrates this scenario for the body model exposed to the antenna.

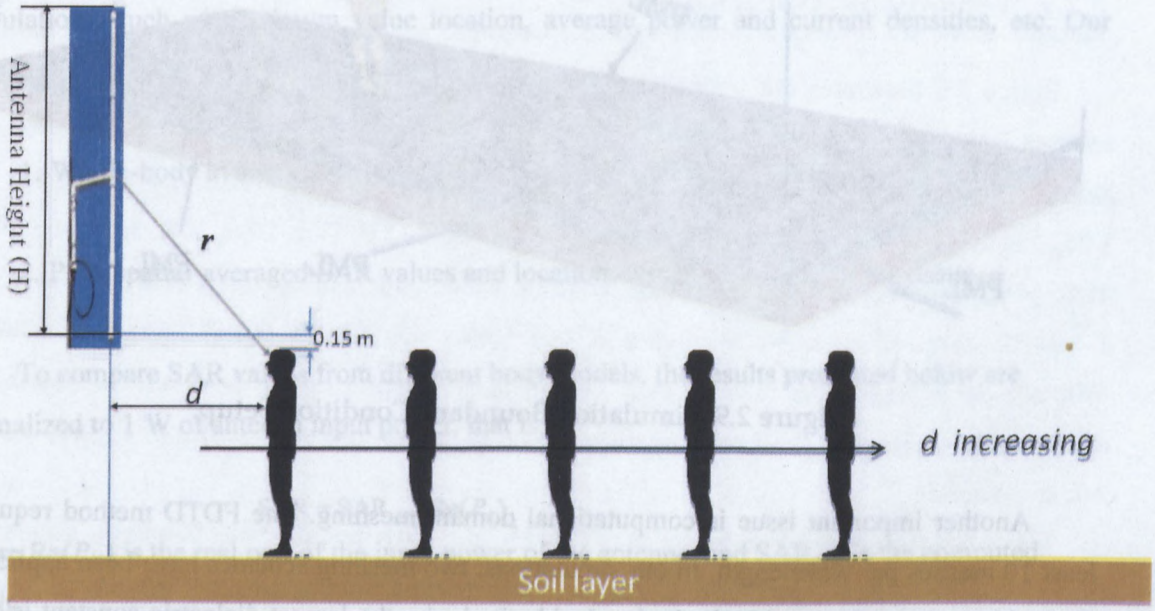

Figure 2.8 The Simulation Setup, in which the Body Model was Positioned Facing the Antenna. The slant distance *r* is from the antenna centre to the body head.

If the body model is moved more than a few tens of metres from the antenna, the simulation domain becomes very large, and requires extremely large computational resources. Therefore,

appropriate boundary conditions must be applied to limit the computational domain. Figure 2.9 shows the boundary condition setup. A resistive sheet boundary (not shown) with an air intrinsic impedance of 377 Ω was applied to the top of the computation domain (+ z wall), representing the top part of the structure exposed to air. PML boundaries with 6-layers have been applied to the other five boundaries of the computational domain.

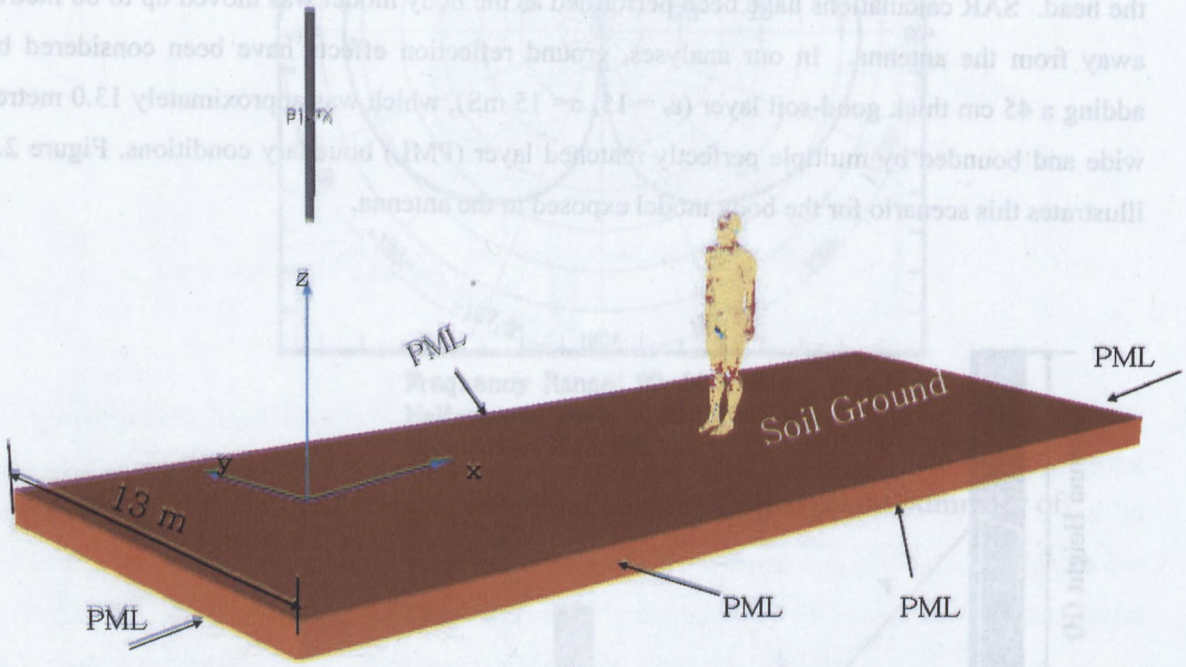

Figure 2.9 Simulation Boundary Condition Setup.

Another important issue is computational domain meshing. The FDTD method requires at least 10 meshes per wavelength. In our simulations, two meshing schemes have been applied, one for inside and one for outside the body. Inside the body, the largest dielectric constant is for the kidneys (98.01 at 100 MHz), and the shortest wavelength (λ_g) is thus 30 cm. However, the mesh size is chosen to match the 'cell' dimensions used for MRI body description, namely 2 mm. This is the voxel size used for all body models, small enough to meet all accuracy requirements.

To achieve stability and convergence, experimentation has included increasing the number of simulation timesteps, reducing the maximum energy level (left inside the structure) to a minimum of -70 dB in most cases. However, all such efforts result in longer computational times. For

example, with a 2009 Dell Precision T7400 Workstation (Quad Core Xeon) on a Linux 64-bit operating system, a typical simulation time for the adult model a few tens of metres from the antenna is about one day, with time increasing to one and half days for horizontal distances beyond 40 metres.

The convergence of the numerical solution has been verified by checking the behaviour of calculated reflection coefficients, input impedance and transmitted power over the operating range of 90-105 MHz.

2.5 SAR Calculation

SAR calculations have been made according to IEEE Standard C95.3-2002 (R2008) [7]. Iteration and interpolation techniques are employed to obtain 1- or 10-g of tissue mass, and peak-spatial and average SAR values. Empire software also provides other options for SAR calculations, such as maximum value location, average power and current densities, etc. Our calculations and analyses are mainly focused on:

1. Whole-body average SAR over a 1- and 10-gram mass.

2. Peak spatial-averaged SAR values and locations over 1- and 10-g of the tissue.

To compare SAR values from different body models, the results presented below are normalized to 1 W of antenna input power, that is

$$\mathrm{SAR} = \mathrm{SAR}_{cal} / \mathrm{Re}(P_{in}),$$

where $\mathrm{Re}(P_{in})$ is the real part of the input power of the antenna, and SAR_{cal} is the computed result.

3. Numerical Results

3.1 Introduction

The vertical 100 MHz antenna was placed in turn facing the BL and MRI body models, at 15 cm above head height. Whole-body average SAR values over 1- and 10-gram mass were calculated as each model was moved away from the antenna. With the maxima location feature and voxel editor of Empire software, peak spatial-averaged SAR values and their tissue locations were obtained. All results are for the antenna input power normalized to 1 W, unless specially mentioned.

3.2 Results for MRI Adult Male Body

3.2.1 Whole-Body Average SAR

Figure 2.9 illustrates the setup for the MRI adult male body model (Duke) exposed to the antenna. The body model was first placed almost under the antenna (d = 0.25 m) and gradually moved away, up to 60 metres, to a total of twenty-eight locations (d = 0.25, 0.50, 0.75, 1.0, 1.5, 1.75, 2.0, 2.25, 2.5, 2.75, 3.0, 4.0, 5.0, 6.0, 8.0, 10.0, 12.5, 15.0, 17.5, 20.0, 25.0, 30.0, 35.0, 40.0, 45.0, 50.0, 55.0 and 60 metres). At each location, whole-body average SAR was calculated over 1- and 10-grams of tissue. No difference in SAR values was noted between the two calculations. Whole-body average SAR values were plotted as a function of the body-antenna horizontal distance d, as shown in the linear-logarithmic and logarithmic-decibel scales of Figures 3.1 and 3.2, respectively.

For a resonant half-wave dipole at 100 MHz, the near-field/far-field boundary occurs at a radius of approximately 120 cm from the centre terminals. At the closest distance used in the simulations (d = 25 cm), analytical models for dipole radiation plus a slab geometry for the body model, indicate that far-field incidence occurs over the lower half of the body. However the power contribution is negligible at these wide angles, compared to near-field contributions over the upper half of the body. Near-field radiation down to the top (head and shoulders) of the body is about twice frontal radiation. As the distance d increases to 50 cm, far-field incidence occurs over most of the torso, but with a continuing negligible contribution to the power. A significant

drop occurs in near-field incidence on the top of the body, with a lesser drop in frontal radiation. At 75 cm, only the head remains in the near-field, however, these contributions still dominate the incident power. At 100 cm, the entire body is in the far-field, a change in the slope of the SAR/distance curve occurs, with a five-fold increase in the far-field contribution, as the body moves 'more into the main beam'. At 150 cm, the further movement into the beam compensates for the increased distance from the dipole, and the incident power is little changed. Beyond this distance, the fall-off with increase in distance, starts to dominate. Slope changes because of soil reflection are also seen in the far-field in Figures 3.1 and 3.2. In Section 3.7 a more detailed discussion is given comparing SAR values with and without the soil.

The behaviour of SAR with distance can be characterized by two distinct intervals of horizontal distance. The first interval starts in the antenna near-field, with a gradual transition to a total far-field by the end of the interval. More detailed discussions about this characterization are given in Chapter 4. To quantify the results, a linear fit has been used with a logarithmic scale coordinate system, and two piecewise approximate expressions obtained for these distance intervals. They are displayed in Figure 3.2. These expressions are:

$$SAR_{ave} = \begin{cases} -6.0635 \times \log_{10} d - 8.2277 & 0.25 \leq d \leq 6.0 \\ -17.004 \times \log_{10} d + 0.35506 & d > 6.0 \end{cases} \tag{3.1}$$

where SAR_{ave} is in dB(mW/kg), and d is in metres.

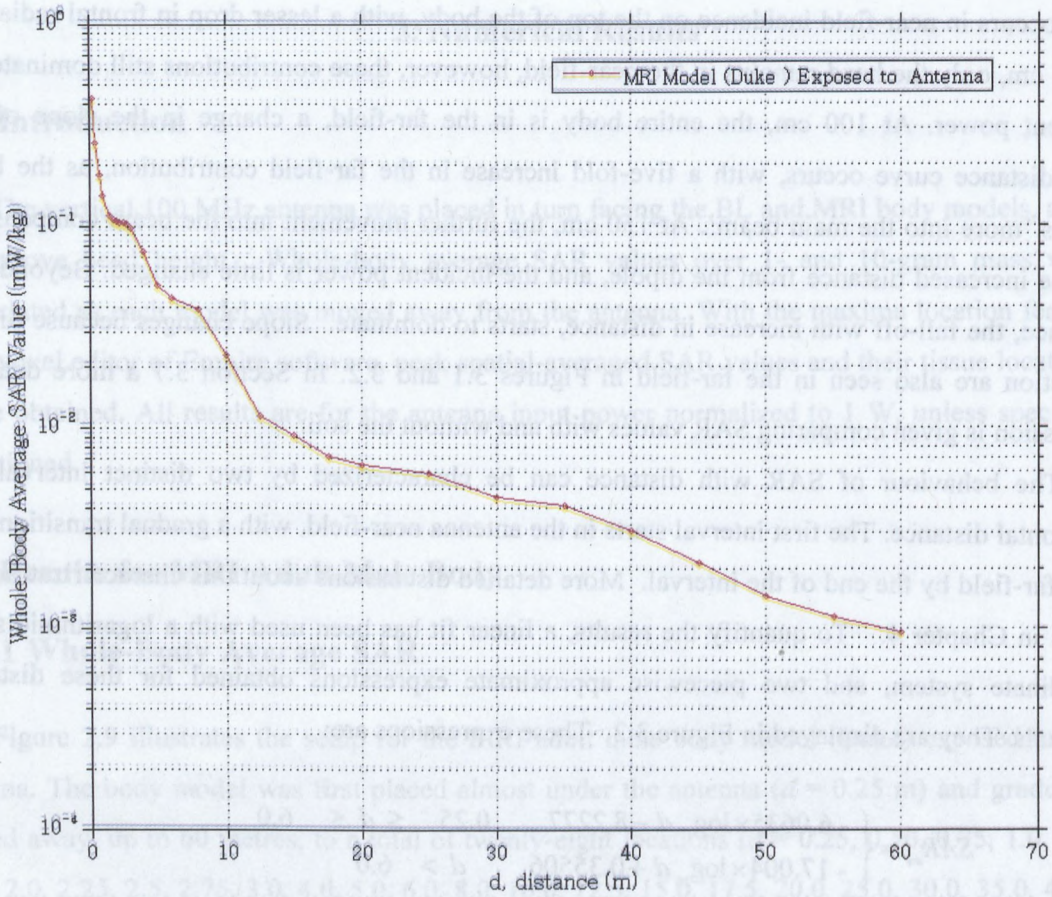

Figure 3.1 Whole-Body Average SAR Values Versus Body-Antenna Horizontal Distance *d*, for an MRI Adult Male (Duke) Exposed to the Antenna at 100 MHz, plotted in linear-logarithmic scale.

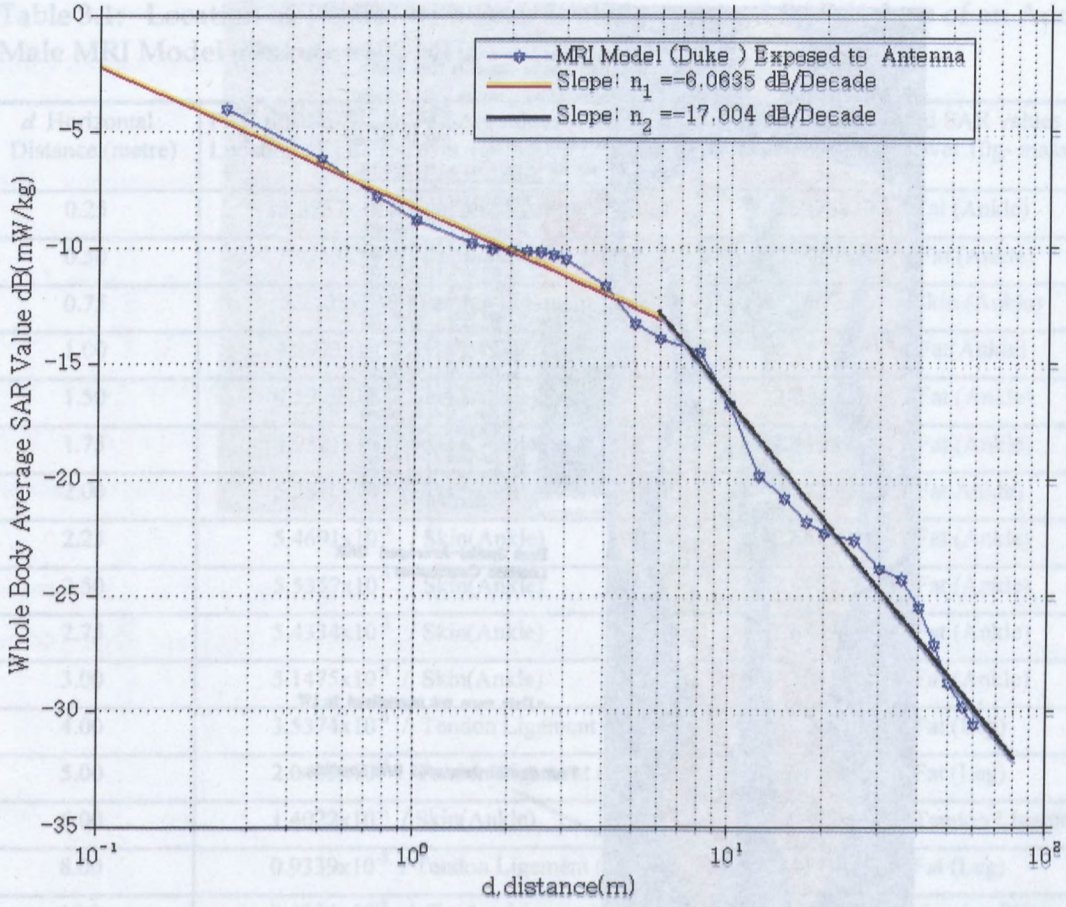

Figure 3.2 Whole-Body Average SAR Values Versus Body-Antenna Horizontal Distance *d*, for an MRI Adult Male (Duke) Exposed to the Antenna at 100 MHz, plotted in logarithmic-decibel scale, and two-segment piecewise linear fitting approximations.

3.2.2 Peak Spatial-Averaged SAR

At each distance *d*, the peak spatial-averaged SAR for the whole body was calculated over 1 g and 10 g. Locations of tissue with peak values were determined using the Empire voxel editor. Table 3.1 summarizes these values and locations. One example of the SAR value distribution, on the cross-section with peak value, is presented in Figure 3.3.

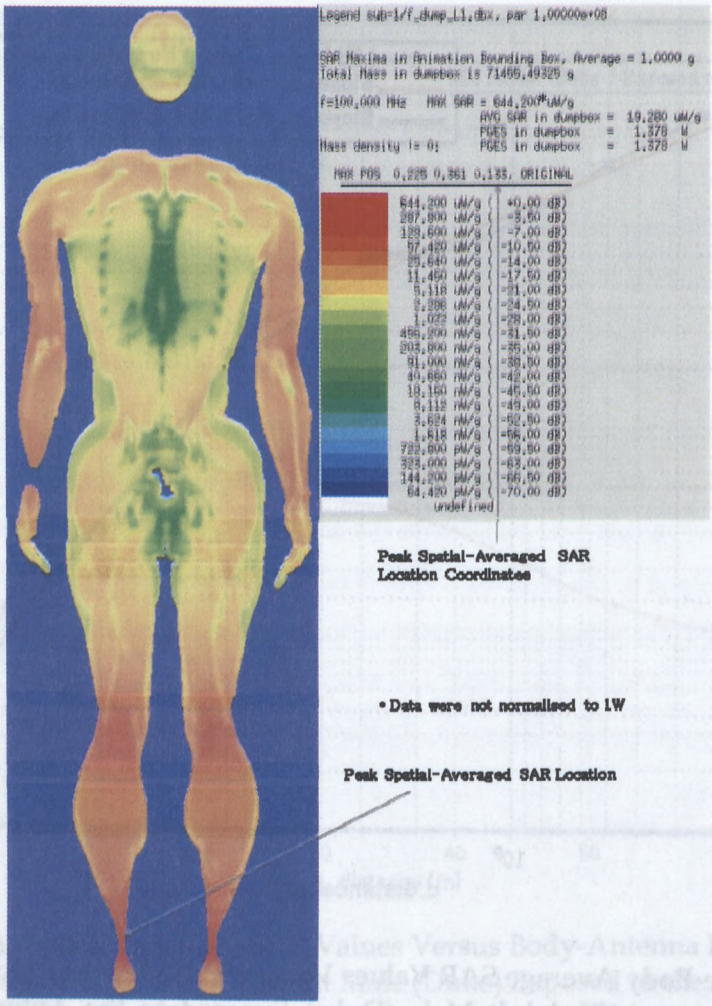

Figure 3.3 SAR Value Distribution 2 mm mesh size, on the cross-section with the peak value at d= 0.25 metres, in which the location of peak spatial-averaged SAR value is marked on the leg. Data presented here are not normalized to 1W of input power of the antenna.

The results in Table 3.1 show that: (1) peak SAR values averaged over 1 g-mass are larger than those over 10 g-mass, as expected. (2) Tissues with peak SAR values always occur in the leg or foot tissues. SAR levels, as discussed in [1, 15] and Section 4.2.1, vary approximately inversely with the body average thickness. The lower body (leg or foot) has a smaller average thickness than other parts of the body. This, in all likelihood, accounts for the location of peak spatial-averaged SAR values in the leg or foot.

Table 3.1: Location of Tissues with Peak Spatial-Averaged SAR Values of an Adult Male MRI Model (Duke) at 100 MHz

d Horizontal Distance (metre)	Peak Spatial-Averaged SAR values (W/kg) and Location of Tissues, over 1g- mass	Peak Spatial-Averaged SAR values (W/kg) and Location of Tissues, over 10g- mass
0.25	13.3737×10^{-3} /Tendon Ligament (Ankle)	6.6973×10^{-3} / Fat (Ankle)
0.50	7.9733×10^{-3} / Tendon Ligament (Ankle)	4.0281×10^{-3} / Fat (Ankle)
0.75	5.2405×10^{-3} / Tendon Ligament (Ankle)	2.6826×10^{-3} / Skin (Ankle)
1.00	4.2973×10^{-3} / Fat (Ankle)	2.1570×10^{-3} / Fat(Ankle)
1.50	4.5979×10^{-3} / Fat (Ankle)	2.2510×10^{-3} / Fat (Ankle)
1.75	4.9521×10^{-3} / Skin(Ankle)	2.4198×10^{-3} / Fat (Ankle)
2.00	5.2816×10^{-3} / Tendon Ligament (Ankle)	2.5723×10^{-3} / Fat Ankle)
2.25	5.4691×10^{-3} / Skin(Ankle)	2.6661×10^{-3} / Fat (Ankle)
2.50	5.5357×10^{-3} / Skin(Ankle)	2.6954×10^{-3} / Fat (Ankle)
2.75	5.4334×10^{-3} / Skin(Ankle)	2.6463×10^{-3} / Fat (Ankle)
3.00	5.1475×10^{-3} / Skin(Ankle)	2.5032×10^{-3} / Fat (Ankle)
4.00	3.5374×10^{-3} / Tendon Ligament (Leg)	1.7200×10^{-3} / Fat (Leg)
5.00	2.0405×10^{-3} / Tendon Ligament (Leg)	1.0117×10^{-3} / Fat (Leg)
6.00	1.4022×10^{-3} / Skin(Ankle)	0.6965×10^{-3} / Tendon Ligament (Ankle)
8.00	0.9339×10^{-3} / Tendon Ligament (Leg)	0.4491×10^{-3} / Fat (Leg)
10.0	0.4354×10^{-3} / Tendon Ligament (Leg)	0.2388×10^{-3} / Muscle of Knee
12.5	0.1483×10^{-3} / Muscle close to Hand	0.0942×10^{-3} / Muscle of Knee
15.0	0.1799×10^{-3} / Tendon Ligament (Leg)	0.0875×10^{-3} / Muscle of Knee
17.5	0.2025×10^{-3} / Tendon Ligament (Leg)	0.0984×10^{-3} / Muscle of Knee
20.0	0.1856×10^{-3} / Tendon Ligament (Leg)	0.0900×10^{-3} / Muscle of Knee
25.0	0.1418×10^{-3} / Tendon Ligament (Leg)	0.0686×10^{-3} / Muscle of Knee
30.0	0.0996×10^{-3} Tendon Ligament (Leg)	0.0483×10^{-3} / Muscle of Knee
35.0	0.1001×10^{-3} / Tendon Ligament (Leg)	0.0449×10^{-3} / Muscle of Knee
40.0	0.0754×10^{-3} / Tendon Ligament (Leg)	0.0365×10^{-3} / Muscle of Knee
45.0	0.0509×10^{-3} / Tendon Ligament (Leg)	0.0247×10^{-3} / Muscle of Knee
50.0	0.0352×10^{-3} / Tendon Ligament (Leg)	0.0171×10^{-3} / Muscle of Knee
55.0	0.0286×10^{-3} / Tendon Ligament (Leg)	0.0130×10^{-3} / Muscle of Knee
60.0	0.0286×10^{-3} / Tendon Ligament (Leg)	0.0108×10^{-3} / Back of Knee

3.3 Results for Body-Like Adult Male Body

3.3.1 Whole-Body Average SAR

The BL adult male body model was positioned at a level 15 cm below the antenna. The model was first placed almost under the antenna (d = 0.25 m) and gradually moved away out to 60 metres, for a total of twenty locations (d = 0.25, 0.50, 0.75, 1.0, 2.0, 3.0, 5.0, 7.5, 10.0, 15.0, 17.5, 20.0, 25.0, 30.0, 35.0, 40.0, 45.0, 50.0, 55.0 and 60 metres). At each location, whole-body average SAR was calculated over 1- and 10-grams of tissue. No difference in SAR values was noted between the two calculations. Whole-body average SAR values were plotted as a function of the body-antenna horizontal distance (d), in the linear-logarithmic and logarithmic-decibel scales of Figures 3.4 and 3.5, respectively.

A linear fit has been used in a logarithmic scale coordinate system, with two piecewise approximate expressions obtained for these horizontal distance intervals. They are displayed in Figure 3.5, and are:

$$SAR_{ave} = \begin{cases} -5.4786 \times \log_{10} d - 8.1982 & 0.25 \leq d \leq 10 \\ -17.102 \times \log_{10} d + 3.3645 & d > 10 \end{cases} \tag{3.2}$$

where SAR_{ave} is in dB(mW/kg), d in metres.

A comparison has been made between the computed SAR values for the two adult models. As seen from Figure 3.6, SAR values for the MRI model are lower than those for the BL model for body-to-antenna horizontal distances d in the far-field larger than 5 metres. As discussed in Section 2.2, these two body models have slight differences in their geometries (heights and widths) and significant differences in tissue composition. The MRI body was segmented to yield 84 different tissues and organs, and while BL body is comprised of only 40. Fat and muscle are the two most significant tissues in terms of their amounts and volumes. Both bodies have a similar muscle composition of around 11 %. Their fat compositions are significantly different, around 2.6 % and 8.8 % for the MRI and BL bodies, respectively. Thus fat-to-muscle ratios are significantly different. Analysis shows that whole body average SAR is significantly dependent on subcutaneous fat [12]. At RF frequencies above body resonance, a statistically thicker fat

layer behaves as an impedance matching layer between the external free space and the internal lossy tissues, resulting in larger SAR values [13].

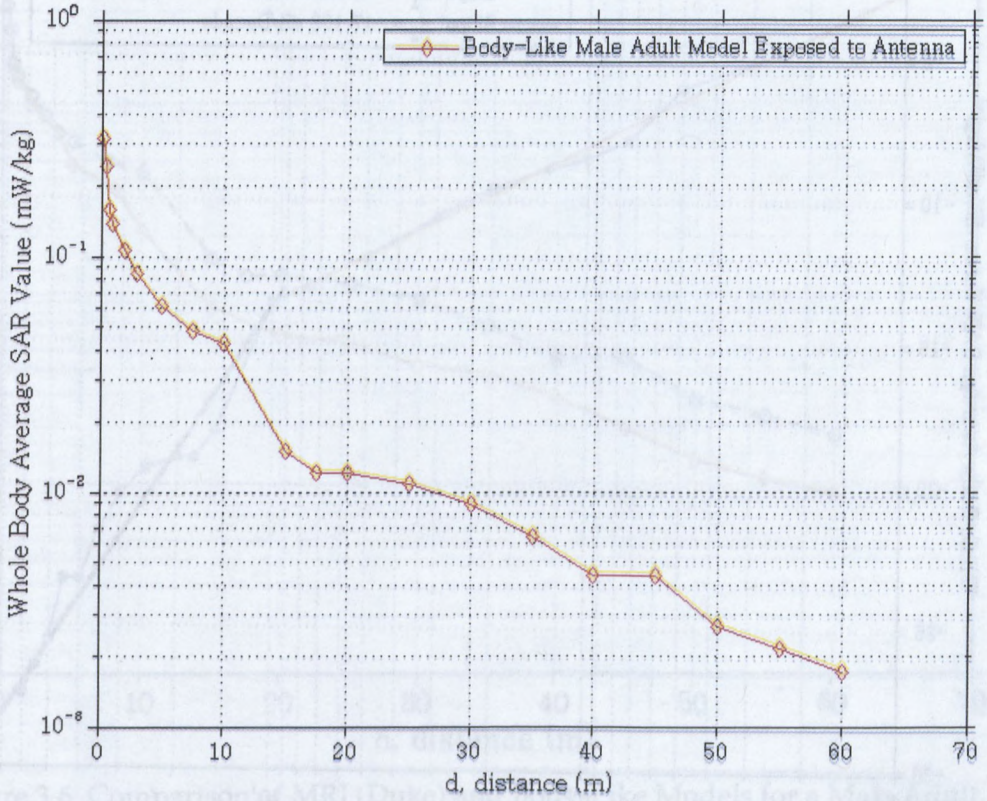

Figure 3.4 Whole-Body Average SAR Values Versus Body-Antenna Horizontal Distance *d*, for an BL Adult Male Exposed to the Antenna at 100 MHz, plotted in linear-logarithmic scale.

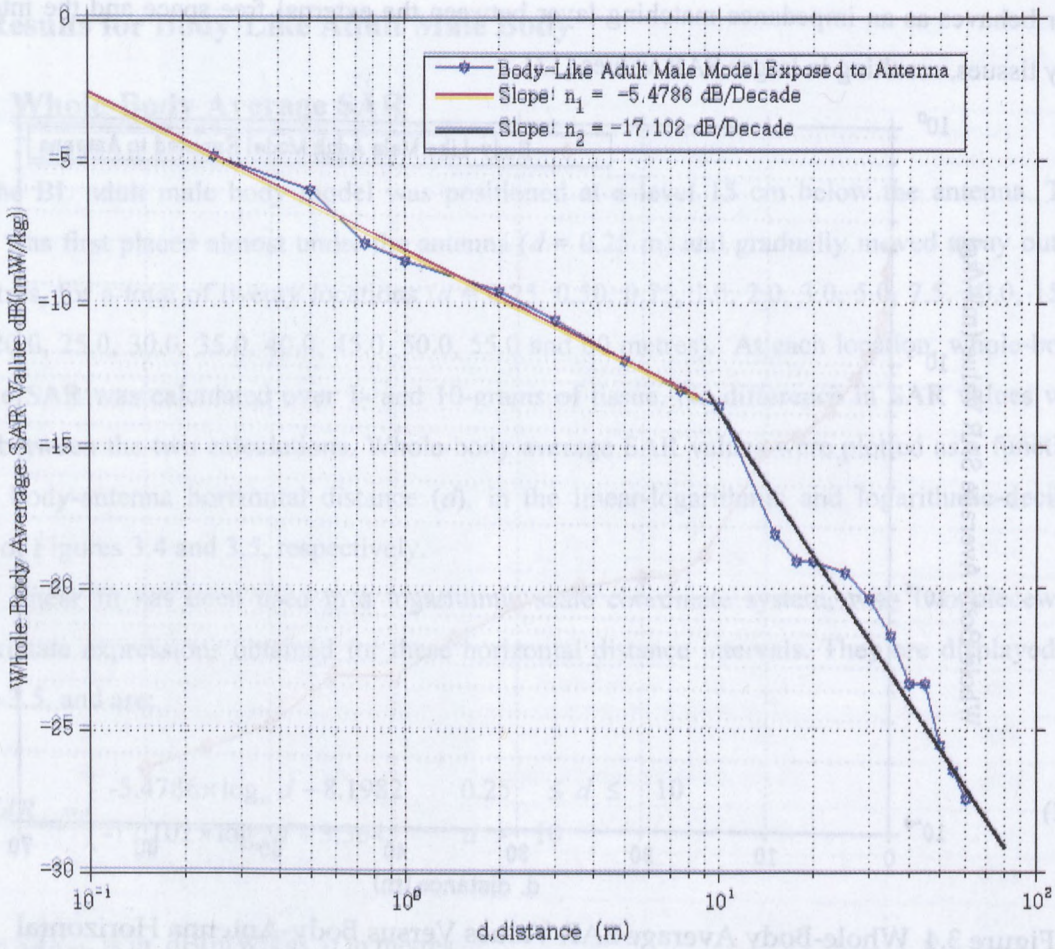

Figure 3.5 Whole-Body Average SAR Values Versus Body-Antenna Horizontal Distance *d*, for a BL Adult Male Exposed to the Antenna at 100 MHz, plotted in linear-logarithmic scale, plotted in logarithmic-decibel scale, and two-segment piecewise linear fitting approximations.

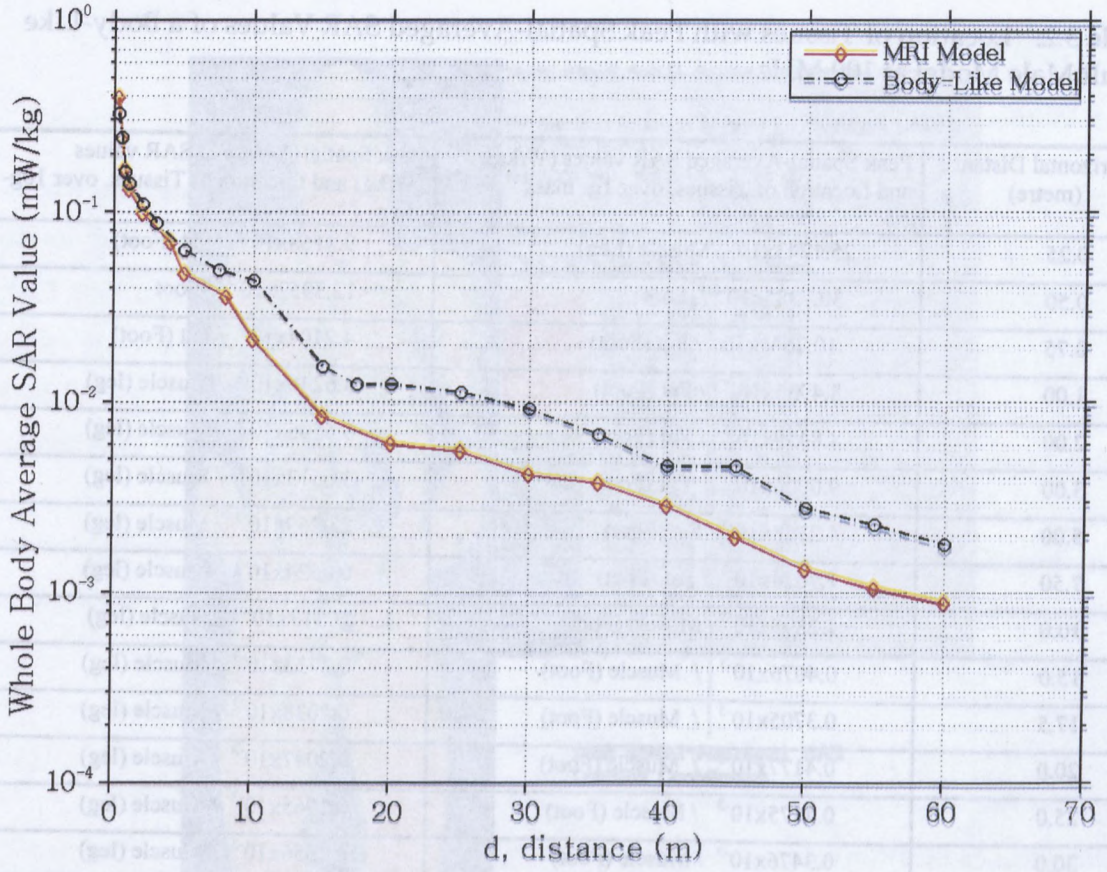

Figure 3.6 Comparison of MRI (Duke) and Body-Like Models for a Male Adult.

3.3.2 Peak Spatial-Averaged SAR

Table 3.2 summarizes peak spatial-averaged SAR values and the locations of tissue for the whole body, over 1 g and 10 g. Again, Table 3.2 shows that locations with peak SAR values occur in the leg or foot. As suggested, this is likely caused by the lower body parts (leg or foot) having a smaller average thickness. An example of the SAR value distribution for the BL model, on the cross-section with the peak SAR value, is presented in Figure 3.7.

Table 3.2: Location of Tissues with Peak Spatial-Averaged SAR Values of a Body-Like Adult Male Model at 100 MHz

d Horizontal Distance (metre)	Peak Spatial-Averaged SAR values (W/kg) and Location of Tissues, over 1g- mass	Peak Spatial-Averaged SAR values (W/kg) and Location of Tissues, over 10g-mass
0.25	25.1243×10^{-3} /Muscle (Leg)	9.8168×10^{-3} / Fat (Foot)
0.50	30.7385×10^{-3} / Foot	12.3952×10^{-3} / Foot
0.75	10.7642×10^{-3} / Fat (Foot)	4.2104×10^{-3} / Fat (Foot)
1.00	8.4936×10^{-3} / Fat (Foot)	3.6240×10^{-3} / Muscle (leg)
2.00	8.8459×10^{-3} / Fat (Foot)	3.6505×10^{-3} / Muscle (leg)
3.00	9.0006×10^{-3} / Fat (Foot)	3.6513×10^{-3} / Muscle (leg)
5.00	4.2798×10^{-3} Fat (Foot)	2.0269×10^{-3} / Muscle (leg)
7.50	1.7074×10^{-3} / Fat (Foot)	0.9524×10^{-3} / Muscle (leg)
10.0	1.2895×10^{-3} Muscle (Foot)	0.7313×10^{-3} / Muscle (leg)
15.0	0.4076×10^{-3} / Muscle (Foot)	0.2753×10^{-3} / Muscle (leg)
17.5	0.3705×10^{-3} / Muscle (Foot)	0.2038×10^{-3} / Muscle (leg)
20.0	0.4177×10^{-3} / Muscle (Foot)	0.2047×10^{-3} / Muscle (leg)
25.0	0.4175×10^{-3} / Muscle (Foot)	0.1965×10^{-3} / Muscle (leg)
30.0	0.3476×10^{-3} / Muscle (Foot)	0.1656×10^{-3} / Muscle (leg)
35.0	0.2606×10^{-3} Muscle (Foot)	0.1261×10^{-3} / Muscle (leg)
40.0	0.1885×10^{-3} / Muscle (Foot)	0.0886×10^{-3} / Muscle (leg)
45.0	0.1483×10^{-3} / Muscle (Foot)	0.0686×10^{-3} / Muscle (leg)
50.0	0.1234×10^{-3} / Muscle (Foot)	0.0577×10^{-3} / Muscle (leg)
55.0	0.1008×10^{-3} / Muscle (Foot)	0.0476×10^{-3} / Muscle (leg)
60.0	0.0803×10^{-3} / Muscle (Foot)	0.0384×10^{-3} / Muscle (leg)

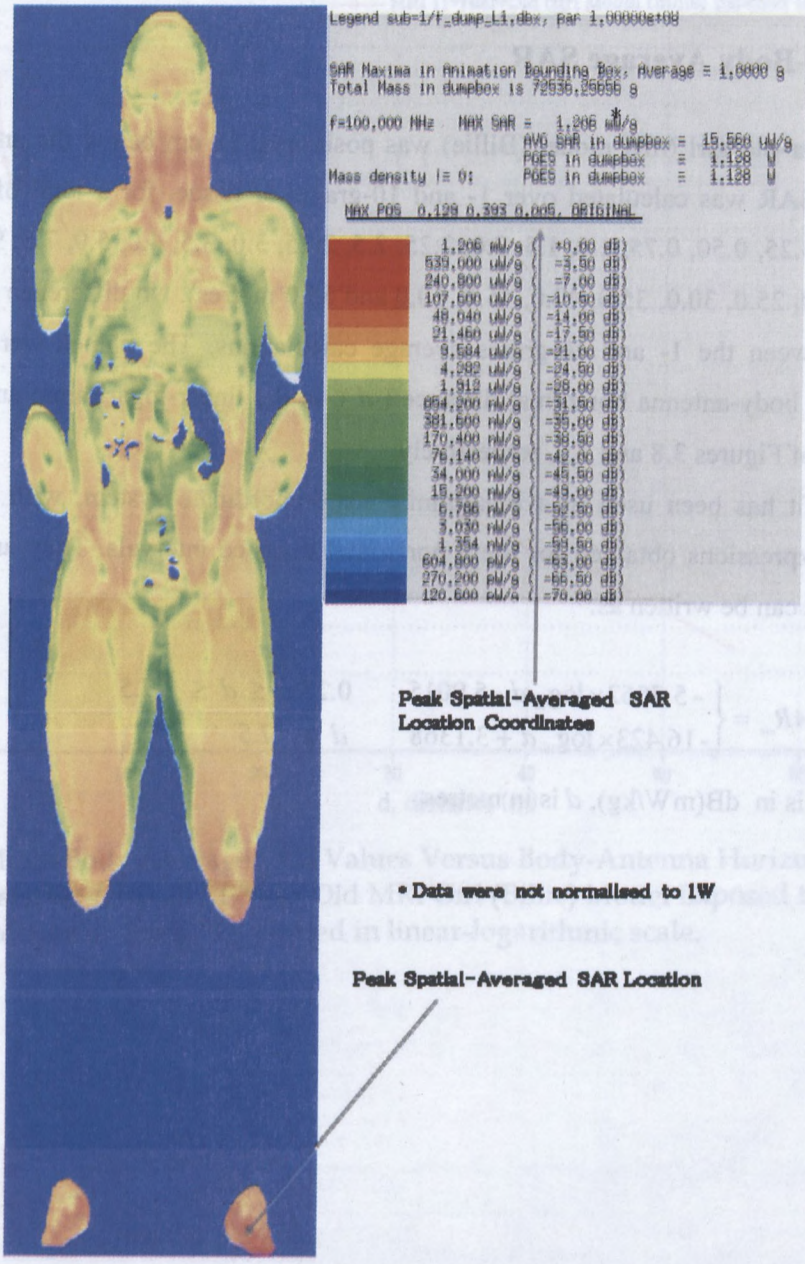

Figure 3.7 SAR Value Distribution 2 mm mesh size, on the cross-section with the peak value at d= 0.25 metres, in which the location of peak spatial-averaged SAR value is marked on the foot. Data presented here are not normalized to 1W of input power of the antenna.

3.4 Results for MRI 11- Year-Old Girl

3.4.1 Whole-Body Average SAR

The 11-year-old girl MRI model (Billie) was positioned 15 cm below the antenna. Whole-body average SAR was calculated over 1- and 10-grams of tissue, for a total of twenty-seven locations (d = 0.25, 0.50, 0.75, 1.0, 1.5, 2.0, 2.25, 2.5, 2.75, 3.0, 3.5, 4.0, 5.0, 7.5, 9.0, 10.0, 12.5, 15.0, 17.5, 20.0, 25.0, 30.0, 35.0, 40.0, 45.0, 50.0 and 55.0 metres). No difference in SAR values was noted between the 1- and 10-grams average calculations. The values were plotted as a function of the body-antenna horizontal distance (d), in the linear-logarithmic and logarithmic-decibel scales of Figures 3.8 and 3.9, respectively.

A linear fit has been used in a logarithmic scale coordinate system, with two piecewise approximate expressions obtained for these horizontal distance intervals. They are displayed in Figure 3.9, and can be written as:

$$SAR_{ave} = \begin{cases} -5.7562 \times \log_{10} d - 5.9015 & 0.25 \leq d \leq 7.5 \\ -16.423 \times \log_{10} d + 3.1368 & d > 7.5 \end{cases} \tag{3.3}$$

where SAR_{ave} is in dB(mW/kg), d is in metres.

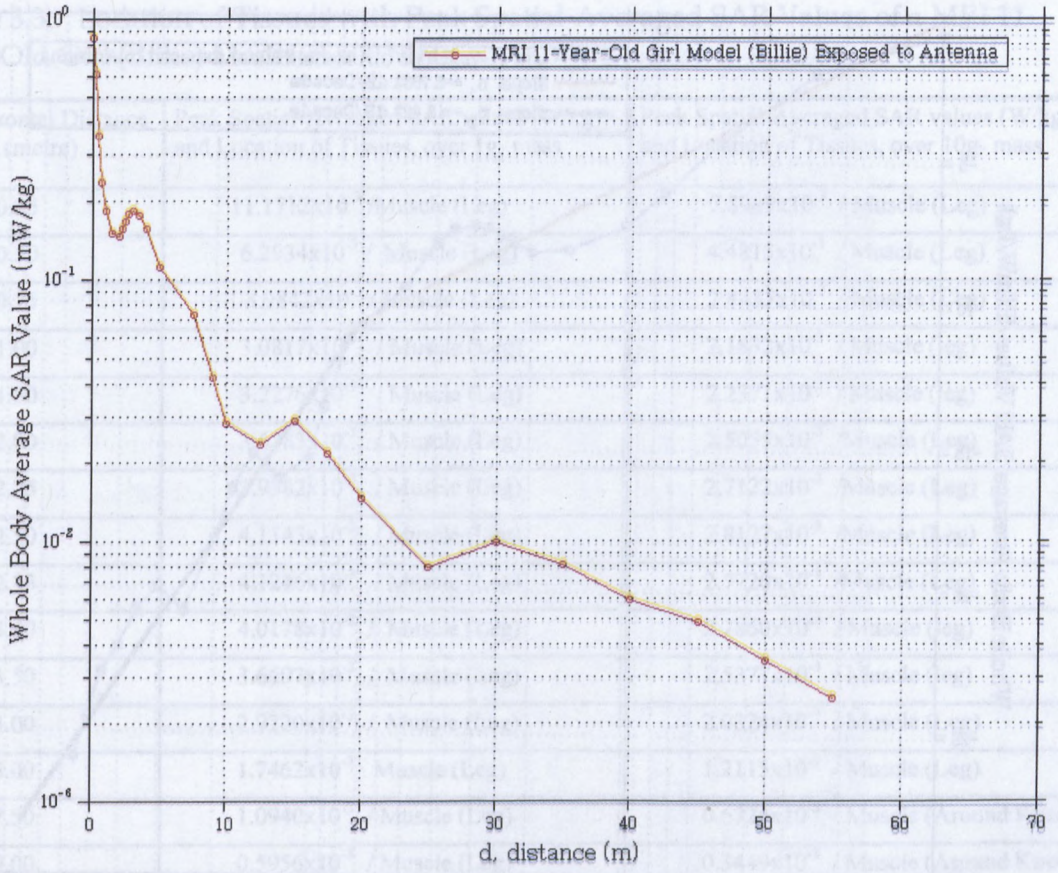

Figure 3.8 Whole-Body Average SAR Values Versus Body-Antenna Horizontal Distance *d*, for an 11-Year-Old MRI Girl (Billie) Model Exposed to the Antenna at 100 MHz, plotted in linear-logarithmic scale.

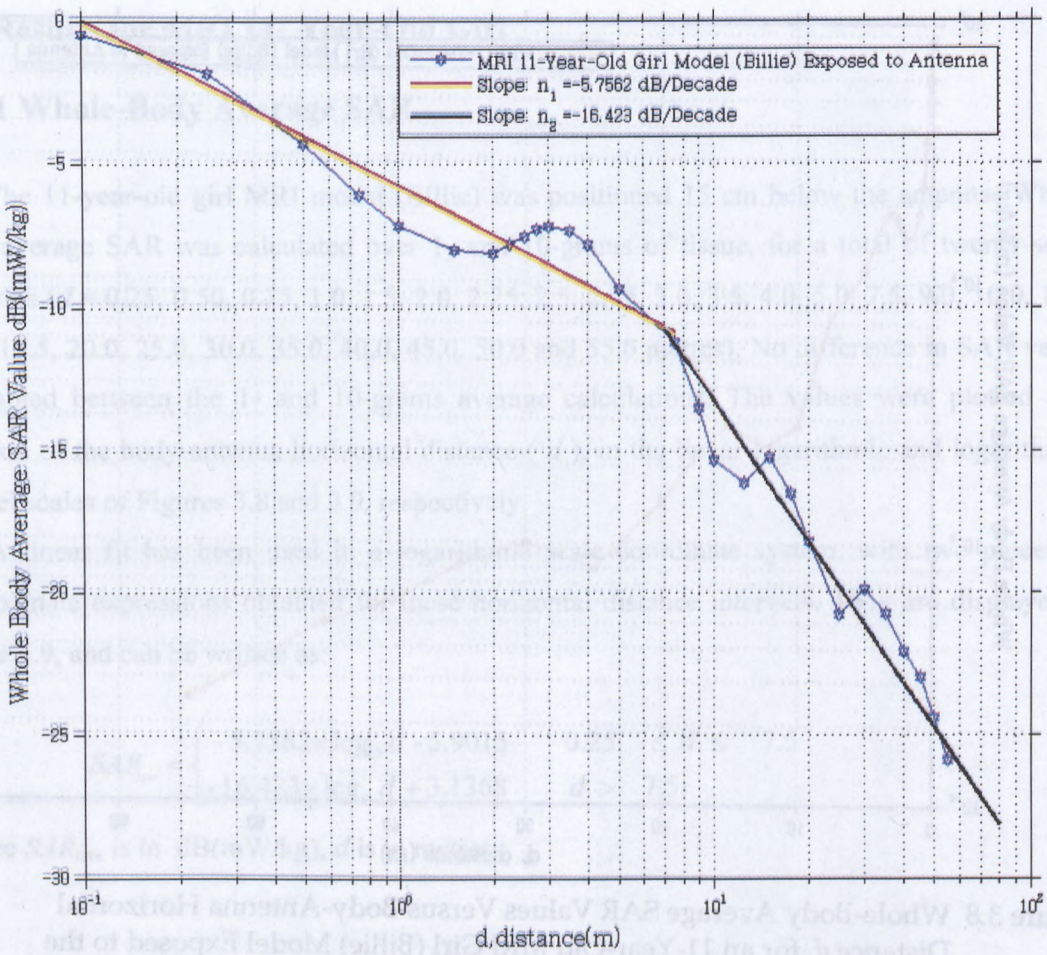

Figure 3.9 Whole-Body Average SAR Values Versus Body-Antenna Horizontal Distance *d*, for an 11-Year-Old MRI Girl (Billie) Model Exposed to the Antenna at 100 MHz, plotted in logarithmic-decibel scale, and two-segment piecewise linear fitting approximations.

3.4.2 Peak Spatial-Averaged SAR

At each distance *d*, peak spatial-averaged SAR values for the whole body was calculated, over 1 g and 10 g. Locations of tissue with peak values were determined with the voxel editor and summarized in Table 3.3. This Table shows that locations with peak SAR values occur in the leg or foot. An example of the SAR value distribution for the girl model, on the cross-section with the peak SAR value, is presented in Figure 3.10

Table 3.3: Location of Tissues with Peak Spatial-Averaged SAR Values of a MRI 11-Year-Old Girl (Billie) Model at 100 MHz

d Horizontal Distance (metre)	Peak Spatial-Averaged SAR values (W/kg) and Location of Tissues, over 1g- mass	Peak Spatial-Averaged SAR values (W/kg) and Location of Tissues, over 10g- mass
0.25	11.1712×10^{-3} /Muscle (Leg)	7.8989×10^{-3} / Muscle (Leg)
0.50	6.2934×10^{-3} / Muscle (Leg)	4.4815×10^{-3} / Muscle (Leg)
0.75	3.9842×10^{-3} / Muscle (Leg)	2.8435×10^{-3} / Muscle (Leg)
1.00	3.0817×10^{-3} / Muscle (Leg)	2.1832×10^{-3} / Muscle (leg)
1.50	3.2276×10^{-3} / Muscle (Leg)	2.2371×10^{-3} / Muscle (leg)
2.00	3.6383×10^{-3} / Muscle (Leg)	2.5055×10^{-3} /Muscle (Leg)
2.25	3.9382×10^{-3} / Muscle (Leg)	2.7122×10^{-3} /Muscle (Leg)
2.50	4.1143×10^{-3} / Muscle (Leg)	2.8127×10^{-3} /Muscle (Leg)
2.75	4.1246×10^{-3} / Muscle (Leg)	2.7720×10^{-3} /Muscle (Leg)
3.00	4.0178×10^{-3} / Muscle (Leg)	2.7860×10^{-3} / Muscle (leg)
3.50	3.6697×10^{-3} / Muscle (Leg)	2.5377×10^{-3} / Muscle (leg)
4.00	2.9220×10^{-3} / Muscle (Leg)	2.0324×10^{-3} / Muscle (Leg)
5.00	1.7462×10^{-3} Muscle (Leg)	1.2115×10^{-3} / Muscle (Leg)
7.50	1.0940×10^{-3} / Muscle (Leg)	0.6724×10^{-3} / Muscle (Around Knee)
9.00	0.5956×10^{-3} / Muscle (Leg)	0.3449×10^{-3} / Muscle (Around Knee)
10.0	0.3617×10^{-3} Muscle (Leg)	0.2125×10^{-3} / Muscle (Around Knee)
12.5	0.3487×10^{-3} Muscle (Leg)	0.2264×10^{-3} / Muscle (Around Knee)
15.0	0.4534×10^{-3} / Muscle (Leg)	0.3061×10^{-3} / Muscle (Around Knee)
17.5	0.3363×10^{-3} / Muscle (Leg)	0.2200×10^{-3} / Muscle (Around Knee)
20.0	0.1187×10^{-3} / Muscle (Leg)	0.1404×10^{-3} / Muscle (Leg)
25.0	0.1181×10^{-3} / Muscle (Leg)	0.0710×10^{-3} / Muscle (Around Knee)
30.0	0.1428×10^{-3} / Muscle (Leg)	0.0872×10^{-3} / Muscle (Around Knee)
35.0	0.1169×10^{-3} Muscle (Leg)	0.0708×10^{-3} / Muscle (Around Knee)
40.0	0.0862×10^{-3} / Muscle (Leg)	0.0525×10^{-3} / Muscle (Around Knee)
45.0	0.0706×10^{-3} / Muscle (Leg)	0.0434×10^{-3} / Muscle (Around Knee)
50.0	0.0503×10^{-3} / Muscle (Leg)	0.0312×10^{-3} / Muscle Around Knee)
55.0	0.0361×10^{-3} / Muscle (Leg)	0.0221×10^{-3} / Muscle (Around Knee)

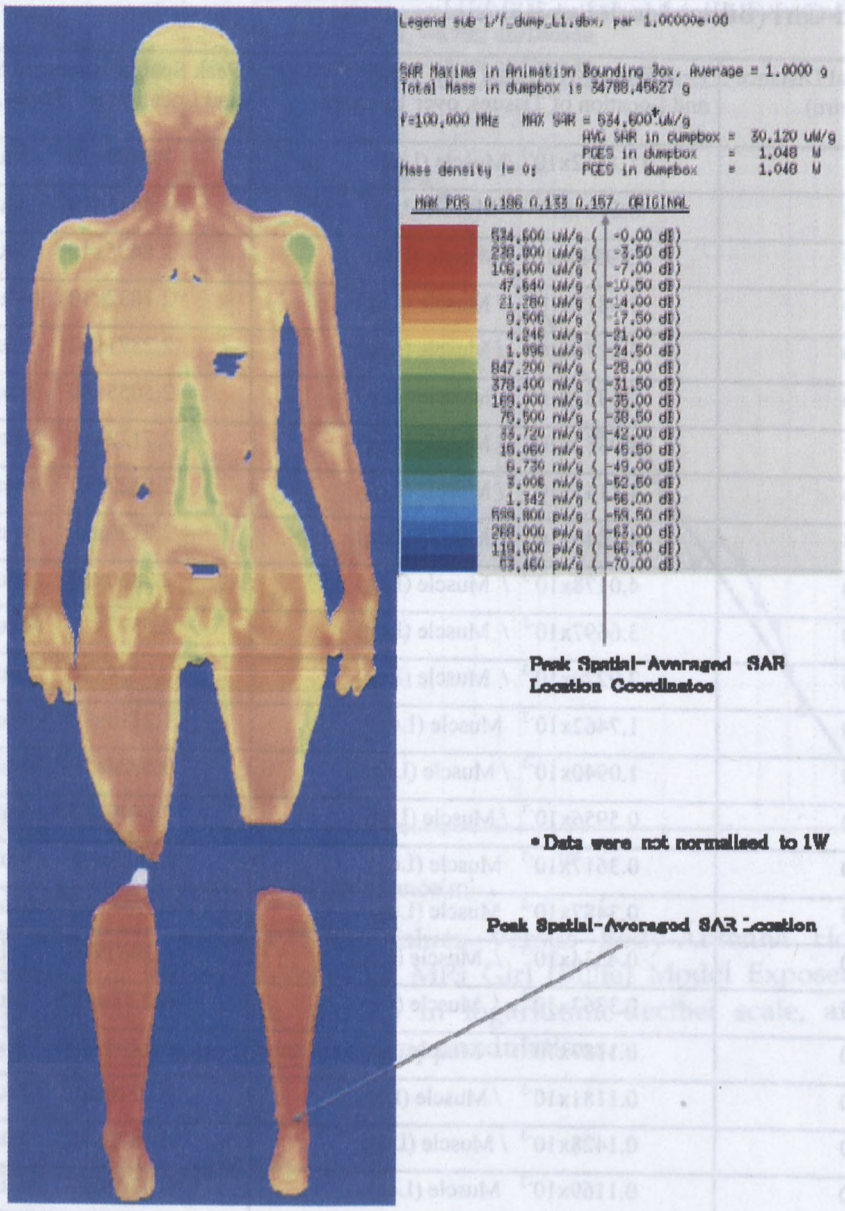

Figure 3.10 SAR Value Distribution 2 mm mesh size for an 11-year-old girl MRI model (Billie), on the cross-section with the peak SAR value at d= 0.25 metres, in which the location of peak spatial-averaged SAR value is marked on the leg. Data presented here are not normalized to 1W of input power of the antenna.

3.5 Results for BL 10-Year Old Boy

3.5.1 Whole-Body Average SAR

The Boy BL Model was exposed to the antenna, and placed in turn at seventeen locations (d = 0.25, 0.5, 0.75, 1.0, 2.5, 5.0, 7.5, 10.0, 15.0, 20.0, 25.0, 30.0, 35.0, 40.0, 45.0, 50.0 and 55.0 metres). Whole-body average SAR values were plotted as a function of the body-antenna horizontal distance d, with the linear-logarithmic and logarithmic-decibel scales of Figures 3.11 and 3.12, respectively.

In a similar fashion, a linear fit has been used in a logarithmic scale coordinate system, with two piecewise approximate expressions obtained for these horizontal distance intervals. They are displayed in Figure 3.12, and can be written as:

$$SAR_{ave} = \begin{cases} -5.8551 \times \log_{10} d - 6.0671 & 0.25 \leq d \leq 7.5 \\ -18.012 \times \log_{10} d + 4.5125 & d > 7.5 \end{cases} \tag{3.4}$$

where SAR_{ave} is in dB(mW/kg), d is in metres.

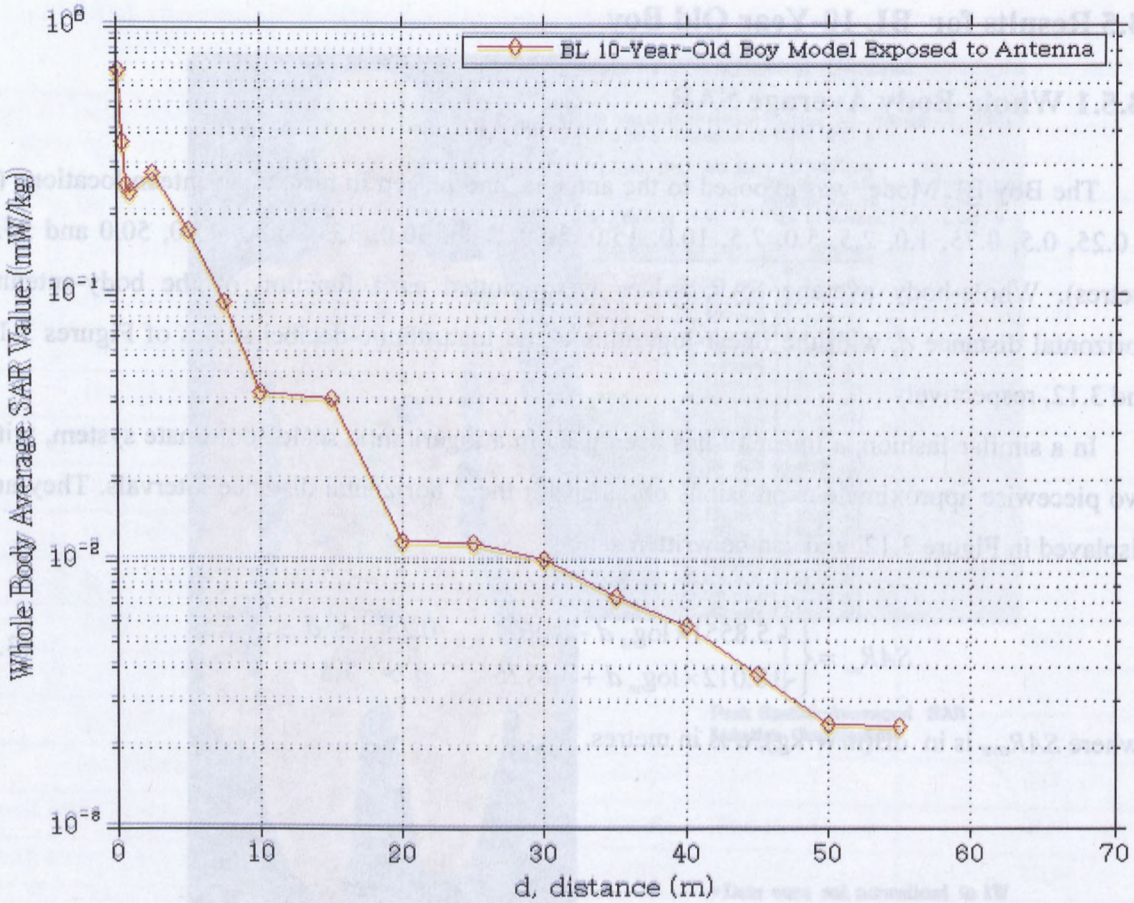

Figure 3.11 Whole-Body Average SAR Values Versus Body-Antenna Horizontal Distance *d*, for a 10-Year-Old BL Boy Model Exposed to the Antenna at 100 MHz, plotted in linear-logarithmic scale.

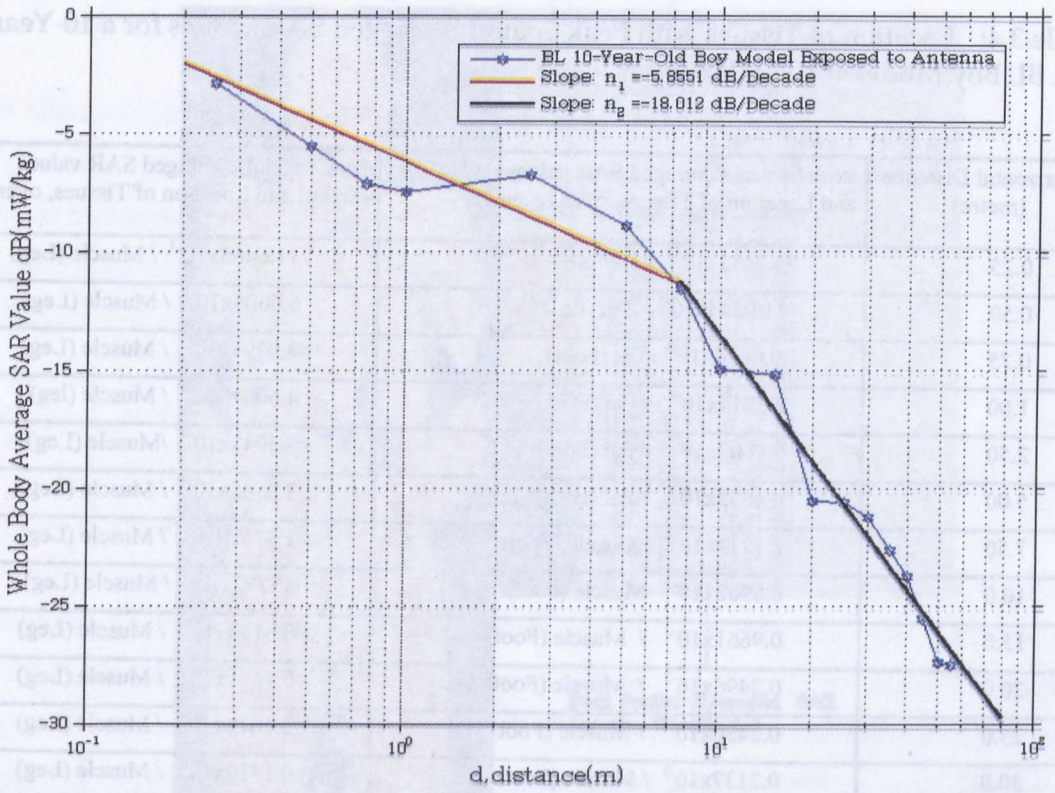

Figure 3.12 Whole-Body Average SAR Values Versus Body-Antenna Horizontal Distance *d*, for a 10-Year-Old BL Boy Model Exposed to the Antenna at 100 MHz, plotted in logarithmic-decibel scale, and two-segment piecewise linear fitting approximations.

3.5.2 Peak Spatial-Averaged SAR

At each distance *d*, peak spatial-averaged SAR values for the whole body were calculated, over 1 g and 10 g. Locations of tissue with peak values were determined with the voxel editor and summarized in Table 3.4. This Table shows that locations with peak SAR values occur in the leg or foot. An example of the SAR value distribution for the Boy Model, on the cross-section with the peak SAR value, is presented in Figure 3.13.

Table 3.4: Location of Tissues with Peak Spatial-Averaged SAR Values for a 10-Year-Old BL Boy Model at 100 MHz

d Horizontal Distance (metre)	Peak Spatial-Averaged SAR values (W/kg) and Location of Tissues, over 1g-mass	Peak Spatial-Averaged SAR values (W/kg) and Location of Tissues, over 10g-mass
0.25	20.7432×10^{-3} /Fat (Foot)	11.6465×10^{-3} / Muscle (Leg)
0.50	11.9844×10^{-3} / Fat (Foot)	6.6608×10^{-3} / Muscle (Leg)
0.75	9.0696×10^{-3} / Fat (Foot)	4.9794×10^{-3} / Muscle (Leg)
1.00	8.3814×10^{-3} / Fat (Foot)	4.6064×10^{-3} / Muscle (leg)
2.50	9.4609×10^{-3} / Fat (Foot)	5.5943×10^{-3} /Muscle (Leg)
5.00	4.4693×10^{-3} / Fat (Foot)	2.8548×10^{-3} / Muscle (Leg)
7.50	2.1211×10^{-3} / Muscle (Foot)	1.3762×10^{-3} / Muscle (Leg)
10.0	0.8902×10^{-3} Muscle (Foot)	0.5772×10^{-3} / Muscle (Leg)
15.0	0.9661×10^{-3} / Muscle (Foot)	0.6140×10^{-3} / Muscle (Leg)
20.0	0.2496×10^{-3} / Muscle (Foot)	0.1671×10^{-3} / Muscle (Leg)
25.0	0.2430×10^{-3} / Muscle (Foot)	0.1618×10^{-3} / Muscle (Leg)
30.0	0.2137×10^{-3} / Muscle (Foot)	0.1419×10^{-3} / Muscle (Leg)
35.0	0.1587×10^{-3} Muscle (Foot)	0.1041×10^{-3} / Muscle (Leg)
40.0	0.1205×10^{-3} / Muscle (Leg)	0.0812×10^{-3} / Muscle (Leg)
45.0	0.0792×10^{-3} / Muscle (Leg)	0.0540×10^{-3} / Muscle (Leg)
50.0	0.0532×10^{-3} / Muscle (Leg)	0.0361×10^{-3} / Muscle (Leg)
55.0	0.0533×10^{-3} / Muscle (Leg)	0.0367×10^{-3} / Muscle (Leg)

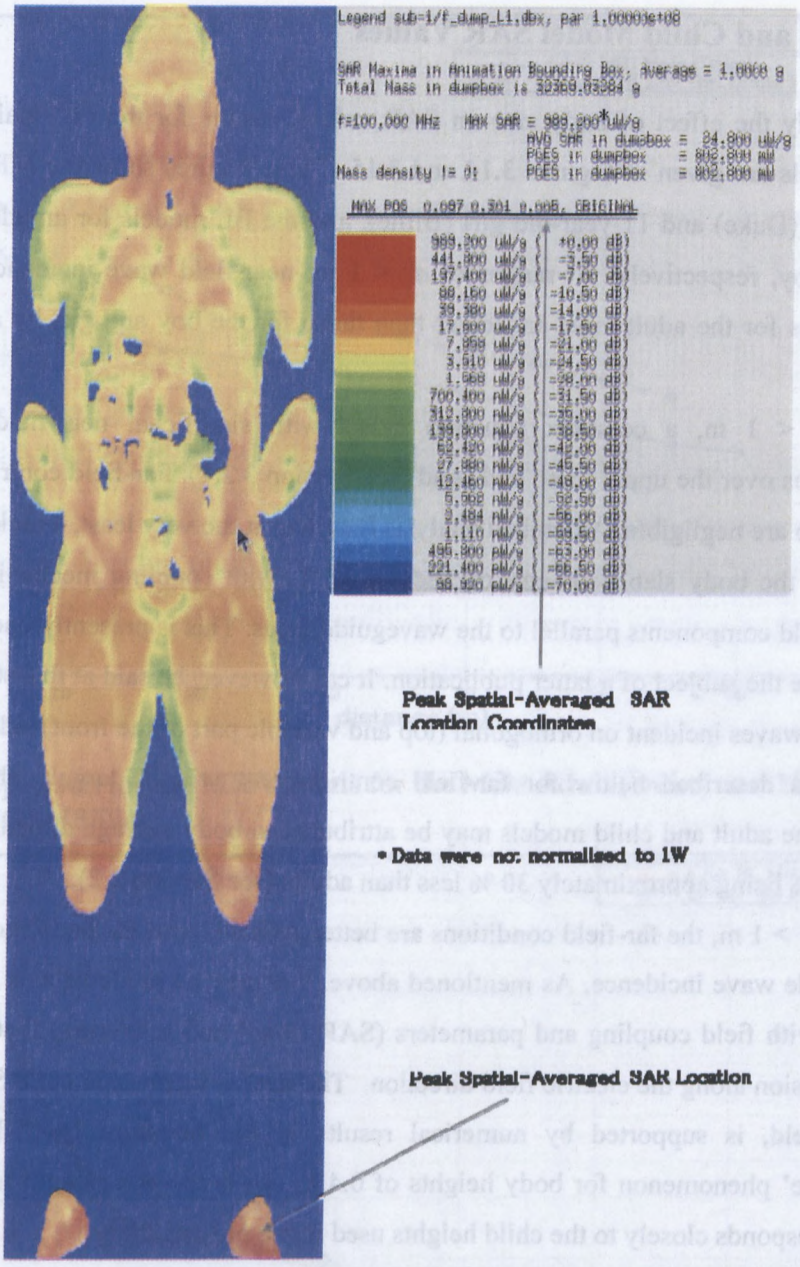

Figure 3.13 SAR Value Distribution 2 mm mesh size for the 10-year-old Boy BL Model, on the cross-section with the peak SAR value at d= 0.25 metres, in which the location of peak spatial-averaged SAR value is marked on the leg. Data presented here are not normalized to 1W of input power of the antenna.

3.6 Adult and Child Model SAR Values

To study the effect of body size on SAR values, results for the two male adult and two child models are given in Figures 3.14 and 3.15. These Figures show the MRI models for an adult male (Duke) and 11-year-old girl (Billie), and the BL models for an adult male and 10-year-old boy, respectively. At ranges of d < 1 m, near-field wave incidence predominates. SAR values for the adult male are lower than those for the boy and girl by a factor between 1.25 and 2.

For d < 1 m, a complex situation exists with significant near-field incident wave distributions over the upper torso and head (see Section 3.2.1). Far-field contributions over the lower torso are negligible. A detailed analysis requires, at the very least, a dielectric waveguide model for the body slab geometry of Section 3.2.1, with coupling mechanisms for incident electric field components parallel to the waveguide faces. This is presently under development, and is to be the subject of a latter publication. It can however, be said at this stage that with the near-field waves incident on orthogonal (top and variable part of the front) sides, the 'resonant' phenomena described below for far-field contributions, will be largely absent. Difference between the adult and child models may be attributed to body average dimensions; child body dimensions being approximately 30 % less than adults (see Section 2.2).

For d > 1 m, the far-field conditions are better defined, with the body moving further into a broadside wave incidence. As mentioned above, this may be modeled as a dielectric receive antenna with field coupling and parameters (SAR 'load' and scattering) that are functions of the dimension along the electric field direction. The further increase in child SAR over adult in the far-field, is supported by numerical results in the literature [14]. These describe a 'resonance' phenomenon for body heights of 0.4 λ_o (λo is the wavelength in free-space)[15]. This corresponds closely to the child heights used in the present study.

However for the boy ranges of d > 10 m, very little difference is found from the BL model for an adult male. The BL boy model was obtained by scaling the BL male adult model [1]. Those data for the BL-boy model require further investigation.

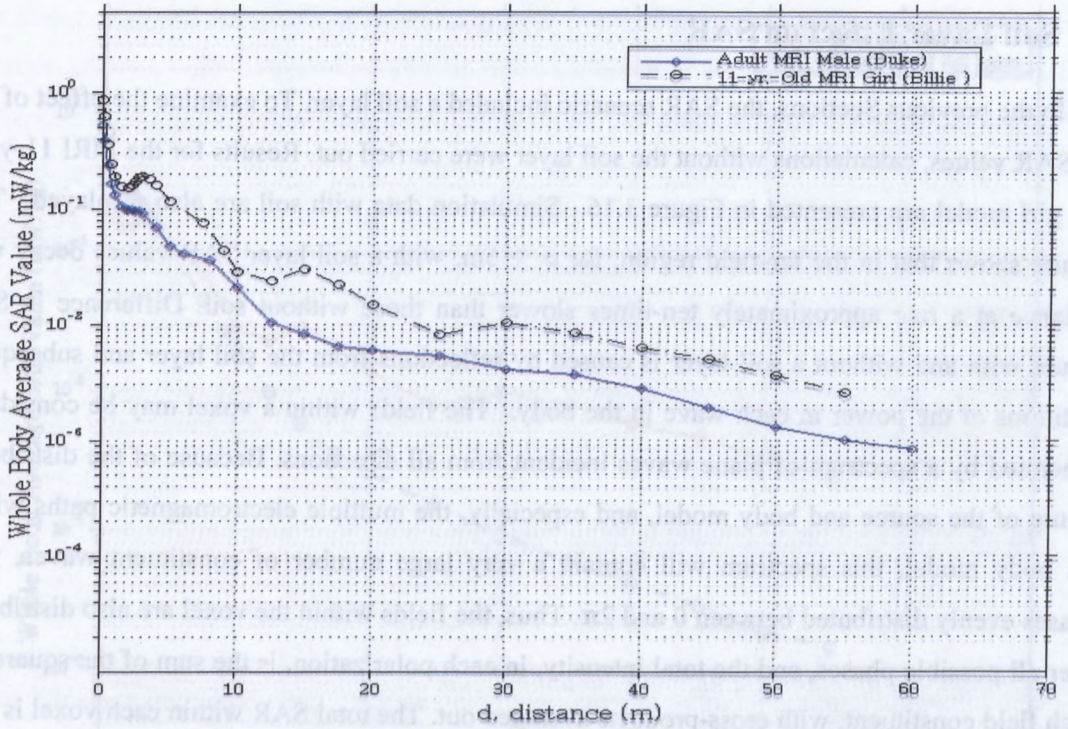

Figure 3.14 Comparison for the MRI models for the Male Adult (Duke) and 11-Year-Old Girl (Billie).

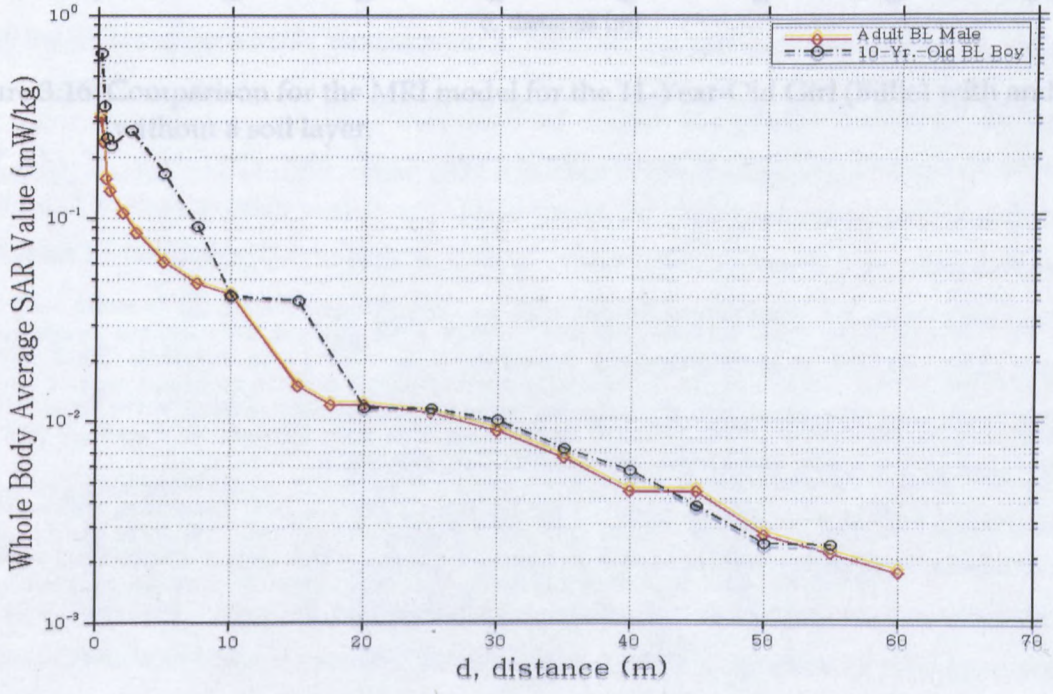

Figure 3.15 Comparison for the BL models for the Male Adult and 10-Year-Old Boy.

3.7 Soil Layer Effect on SAR

In the previous Sections, the SAR scenario included a soil layer. To examine the effect of soil on SAR values, calculations without the soil layer were carried out. Results for the MRI 11-year-old girl model are presented in Figure 3.16. Simulation data with soil are also displayed. This Figure shows that in the far-field region, for $d > 5$m, with a soil layer SAR values decay with distance at a rate approximately ten-times slower than those without soil. Difference in SAR values with and without a soil layer is caused by reflections from the soil layer and subsequent additions of the power in each wave in the body. The fields within a voxel may be considered generated by a spectrum of plane waves incident from all directions. Because of the distributed nature of the source and body model, and especially, the multiple electromagnetic paths within the body model, this spectrum will contain a very large number of constituent waves, with phases evenly distributed between 0 and 2π. Thus, the fields within the voxel are also distributed over all possible phases, and the total intensity, in each polarization, is the sum of the squares of each field constituent, with cross-products averaged out. The total SAR within each voxel is thus the sum of the squares of each field component, positive numbers with no net constructive or destructive interference.

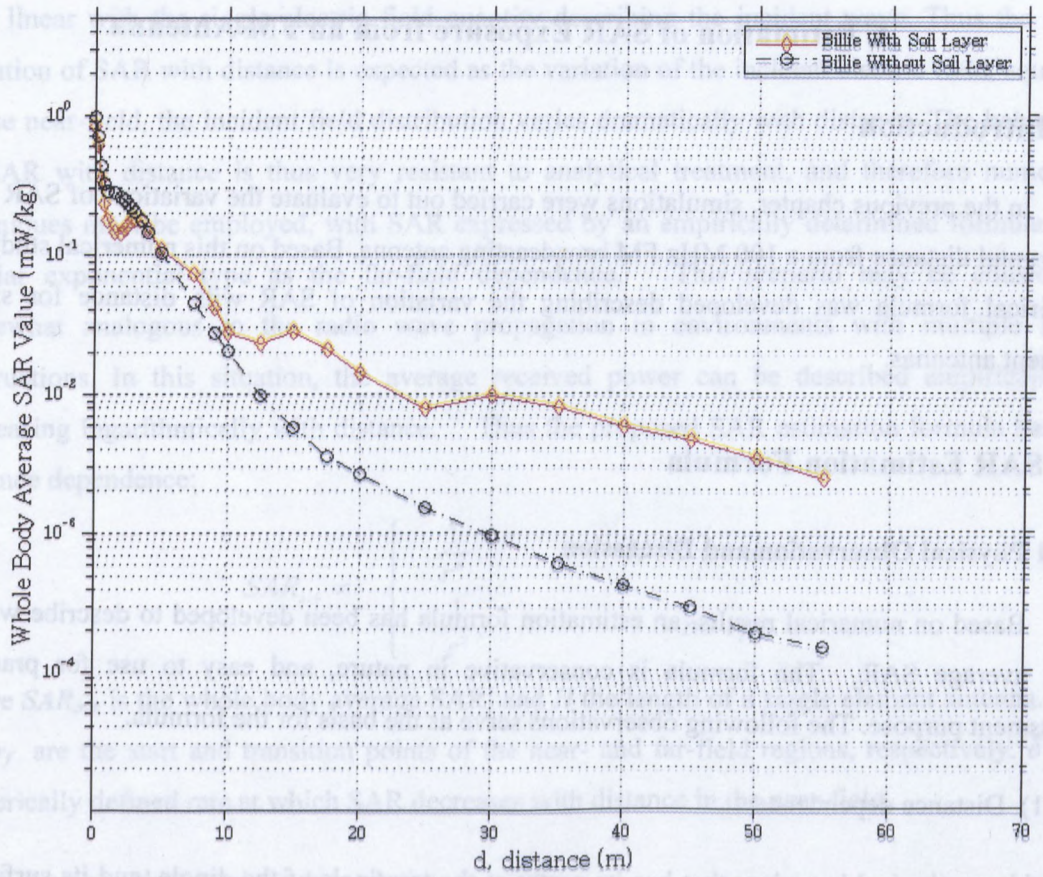

Figure 3.16 Comparison for the MRI model for the 11-Year-Old Girl (Billie) with and without a soil layer.

4. Estimation of SAR Exposure from an FM Antenna

4.1 Introduction

In the previous chapter, simulations were carried out to evaluate the variations of SAR with horizontal distance from a 100 MHz FM broadcasting antenna. Based on this numerical study, an empirical formula was developed describing the variation of SAR with distance for single element antennas.

4.2 SAR Estimation Formula

4.2.1 Physical Observation and Discussion

Based on numerical results, an estimation formula has been developed to describe whole-body average SAR. The formula is conservative in nature, and easy to use for practical assessment purpose. The following observations serve as the basis for the formula.

1) Distance dependence

Outside a spherical boundary that has its centre at the terminals of the dipole, and its surface at the same distance as the antenna ends ($\pm\frac{H}{2}$), an infinite family of spherical waves of the transverse magnetic (TM) type exists. The summation of these constitutes the free wave travelling through space away from the antenna [16]. The electric fields in each of those waves have both radiative and reactive components. In the near-field of the dipole, each of the reactive components varies in a complicated fashion with the slant distance r from the antenna centre (see Figure 2.8). As the near-field/far-field boundary r_f ($\sim 2H^2/\lambda$) is reached, these reactive components have attenuated, and the radiating waves have a close-to-planar wave front with the impedance of free space, and a transverse electric field varying as $1/r$.

Whole-body SAR is calculated as a sum of the squares of electric field quantities, weighted with the conductivity of each voxel. In each voxel, these field quantities have a unique (and complex) relationship with the incident field distribution. In the far-field, the body model faces a uniform plane wave with its unchanging relative distribution of incident electrical field over the widths and distances of interest. With the (approximately) linear media of the voxels, all voxel fields are

thus linear with the single electric field quantity describing the incident wave. Thus the same variation of SAR with distance is expected as the variation of the incident electric field, squared. In the near-field, the incident field distribution varies dramatically with distance. The behaviour of SAR with distance is thus very resistant to analytical treatment, and therefore numerical techniques must be employed, with SAR expressed by an empirically determined formula of a similar exponential type as the far-field dependence. This scenario may be considered somewhat analogous to the radio wave propagation in environments with multiple lossy obstructions. In this situation, the average received power can be described empirically as decreasing logarithmically with distance. Thus the proposed SAR estimation formula has the distance dependence:

$$SAR_{ave} \propto \begin{cases} \frac{1}{r^{\delta}}, & H/2 \le r \le r_f \\ \frac{1}{r^2}, & r > r_f \end{cases} \tag{4.1}$$

where SAR_{ave} is the whole body average SAR, and H the length of a single element antenna. $H/2$ and r_f are the start and transition points of the near- and far-field regions, respectively. δ is a numerically defined rate at which SAR decreases with distance in the near-field.

2) Antenna characteristic dependence

SAR values are directly associated with the level of absorbed power. Beyond the near-field region, this is a function of the direction and beamwidth of the antenna main beam.

3) Size of exposed body

In this study, whole-body average SAR values were obtained for adult male and boy and girl models. The proposed estimation formulas must consider the effect of body size on SAR values. Consider the body as approximated by a rectangular cylinder, filled with material of density ρ and electric parameters ε, μ , and σ, as in Figure 4.1, where w is the width of the body (facing the wave), t body thickness, and h body height. From this model, the power incident on the body is proportional to wh, and the body mass is proportional to wth. It then follows that

$$SAR \doteq Const \frac{wh}{\rho wth} = \frac{Const}{\rho} \frac{1}{t}, \tag{4.2}$$

where *Const* is a constant. SAR levels, from Equation (4.2), will vary approximately with the inverse of body average thickness.

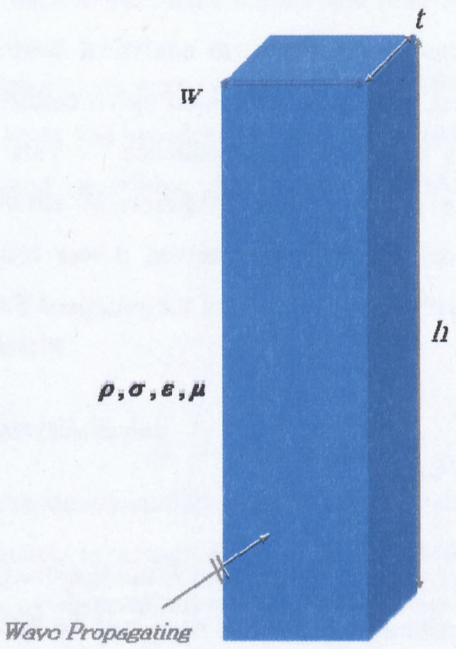

Figure 4.1 Wave Incident on a Rectangular Cylindrical Model for a Body.

4.2.2 Proposed Formula

In a similar fashion to Reference [17], the proposed estimation formula for whole-body average SAR is

$$SAR_{Ave}(r, P_{in}, D_o, \Phi) = \begin{cases} B_1 \kappa \dfrac{P_{in}}{\Phi r^{\delta}}, & H/2 \le d \le d_f \\ B_2 \kappa D_o \dfrac{P_{in}}{\Phi r^2}, & d > d_f \end{cases} \tag{4.3}$$

where

d = horizontal distance from the antenna to the exposed body (metre)

d_f = horizontal transition point of the far-field region (metre).

r = slant distance from the centre of the antenna to the body head (Figure 2.8) (metre)

δ = exponent in the near-field region

P_{in} = antenna input power (Watt)

Φ = vertical half-power beam width (radian) (general antenna)

D_o = vertical directivity of the antenna on soil (dimensionless)

κ = size factor to accommodate different body models (dimensionless)

Referring to the estimation formula given in [17] and based on our simulation data, the transition point to the far-field region d_f, two constants B_1 and B_2 are chosen to give a good fit to numerical data, and a reasonably conservative prediction with respect to SC6 [3] safety levels.

$$B_1 = 10^{-3}\ (kg^{-1}) \text{ and } B_2 = 3/2 \times 10^{-2}\ (kg^{-1}) \tag{4.4}$$

$$d_f = 4 \times \lambda \frac{D_o \Phi}{\pi}\ (m) \tag{4.5}$$

As observed in the previous chapter, the variation of whole-body average SAR with distance decays as $1/r^{\delta}$ ($\delta \approx 0.6$) and approximately as $1/r^2$ in the near- and far- field regions, respectively. The effect of resonance phenomenon for body height has been considered here, because the resonant frequency for humans is between 70 and 100 MHz [15].

The factor κ is approximated by the ratio of body thicknesses. In our simulations, the body thickness of an average male adult was taken as a reference ($\kappa = 1$), and κ value for any other size body thickness can be calculated using Equation (4.2).

4.3 Comparison with Numerical Data

To validate the estimation formula, the values predicted using Equations (4.3) to (4.5) for whole-body average SAR will be compared with numerical data. These data are normalized to 1 W of input power.

4.3.1 Adult Models

For this simulation, the parameters used are:

$\Phi = 104^o$ (or *1.815* radians)

L=1.34 metres (Antenna length)

D_o = *2.14* (dBi) (or 1.636)

κ = *1* for the adult male

δ = 0.6 (from simulation data)

f= 100 MHz

Using Equations (4.3) to (4.5), the estimated whole-body average SAR values for the adult body have been calculated, and plotted in Figure 4.2. The simulation data for the MRI and BL adult models are displayed for comparison.

It is seen that the proposed formula gives a reasonable and conservative approximation to the simulation data.

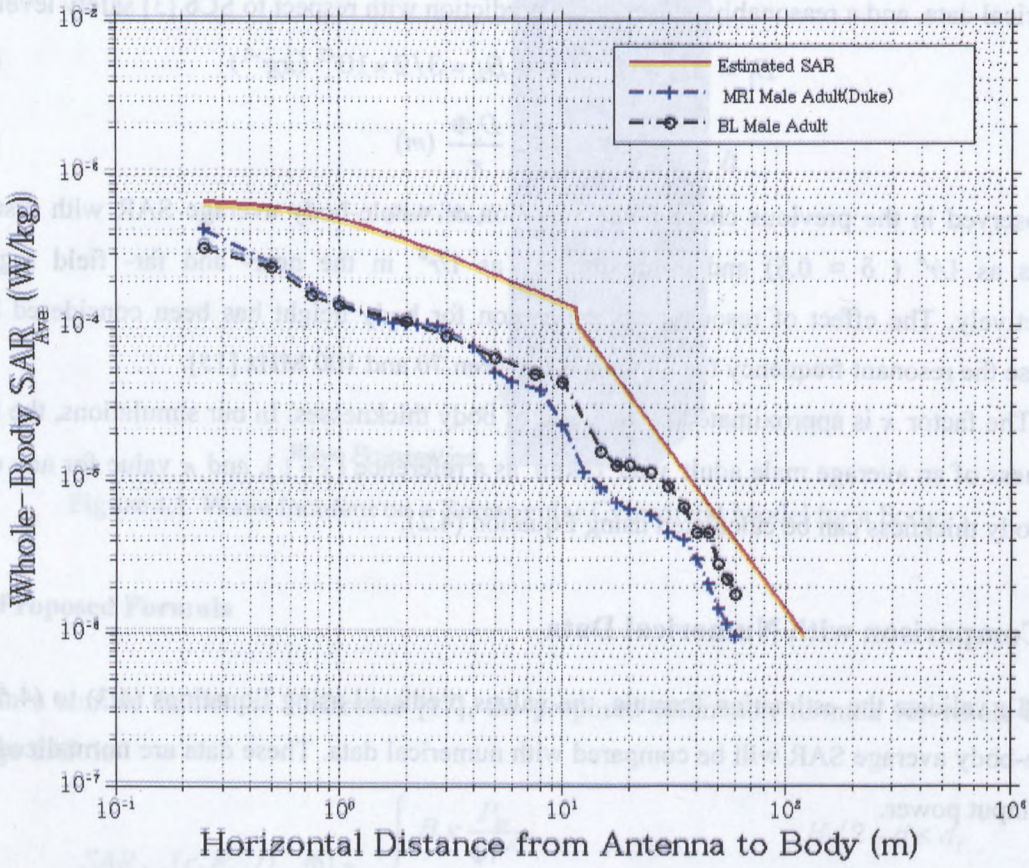

Figure 4.2 Whole-Body Average SAR Values for Adult Male Bodies Compared with the Estimation Formula.

4.3.2 Child Models

As discussed in Section 4.2.1, the size effect is inversely proportional to body average thickness. Examination of the models shows that in average thickness, the body of the 10-year-

old boy or 11-year-old girl is about 30% smaller than an adult male body, resulting in SAR values for these children that are approximately 30% larger than for the adult. Therefore, the size parameter $\kappa = 1.30$ is used in Equation (4.3).

The estimated whole-body average SAR values for the child models have been calculated, and are displayed in Figure 4.3 together with simulation data for the MRI girl and BL boy models. The proposed formula gives reasonable and conservative approximations.

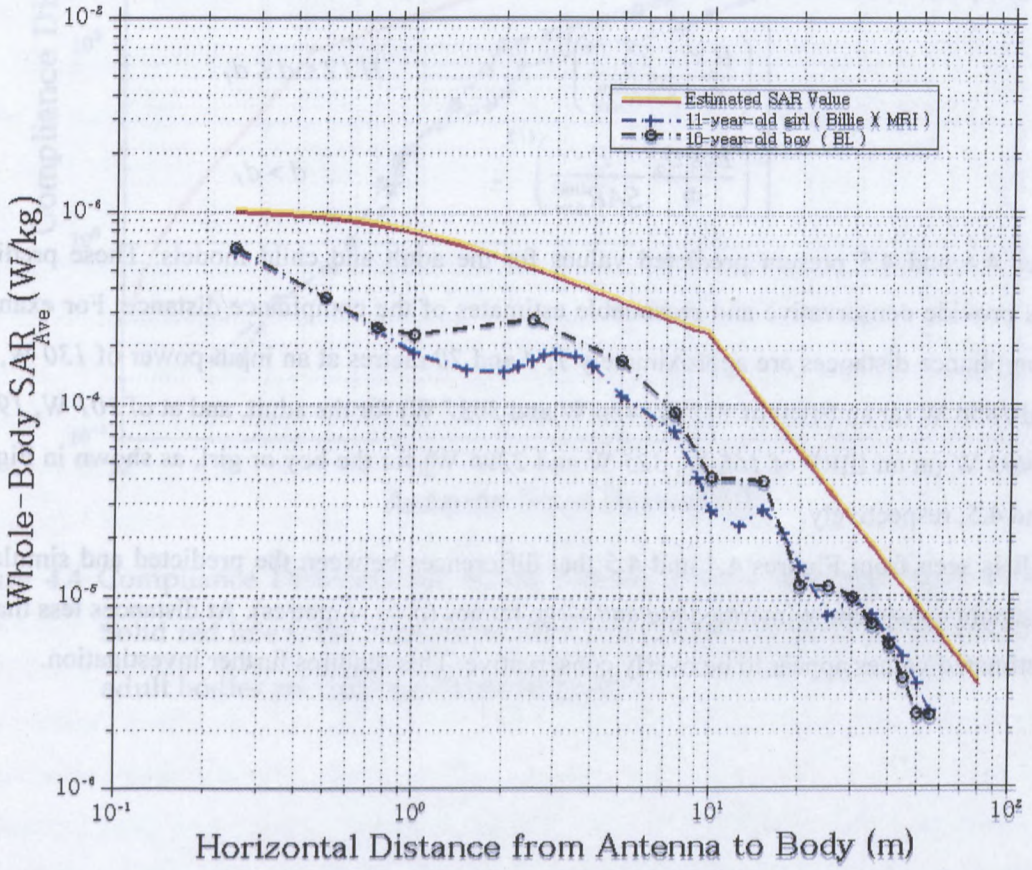

Figure 4.3 Whole-Body Average SAR Values for the Child Models Compared with the Estimation Formula.

4.4 Compliance Distance and Analysis

With the proposed estimation formula, a direct relationship between maximum power density and maximum SAR can be established for compliance with "Limits of Human Exposure

to Radiofrequency Electromagnetic Fields (Health Canada Safety Code 6)" [3], and compliance with the ICNIRP limit of 0.08 (W/kg) (a whole body SAR limit for devices used by the general public). Equation (4.3) can be expressed as a relationship between antenna input power and distance for the limiting SAR value. In previous calculations, all data have been represented in terms of 1 W into the antenna. Let P_c be the required input power to produce the limit value of $SAR_{Ave}^{\lim}(d_c, P_c, D_o, \Phi)$ at the compliance distance d_c. It then follows from Equation (4.3) that the relationship between the compliance distance d_c and input power P_c can be expressed as:

$$d_c = \begin{cases} \left(\dfrac{B_1 \kappa}{\Phi} \dfrac{P_c}{SAR_{Ave}^{\lim}} \right)^{1/\delta}, & H/2 \le d \le d_f \\ \left(\dfrac{B_2 \kappa D_o}{\Phi} \dfrac{P_c}{SAR_{Ave}^{\lim}} \right)^{1/2}, & d > d_f \end{cases} \tag{4.6}$$

Figures 4.4 and 4.5 present predicted values for the adult and child models. These predicted values provide conservative and reasonable estimates of the compliance distance. For example, the compliance distances are approximately *1*, *4* and *20* metres at an input power of *130* W, *260* W and *1856* W (at an EIRP of *212* W, *426* W and *3037* W) for the adult, and at of *101* W, *199* W and *1403* W (at an EIRP of *165* W, *325* W and *2296* W) for the boy or girl, as shown in Figures 4.4 and 4.5, respectively.

It is seen from Figures 4.4 and 4.5 that differences between the predicted and simulation data remain consistent at intermediate and large ranges ($d > 4$ metres). At distances less than d_f, the estimated values appear to be overly conservative. This requires further investigation.

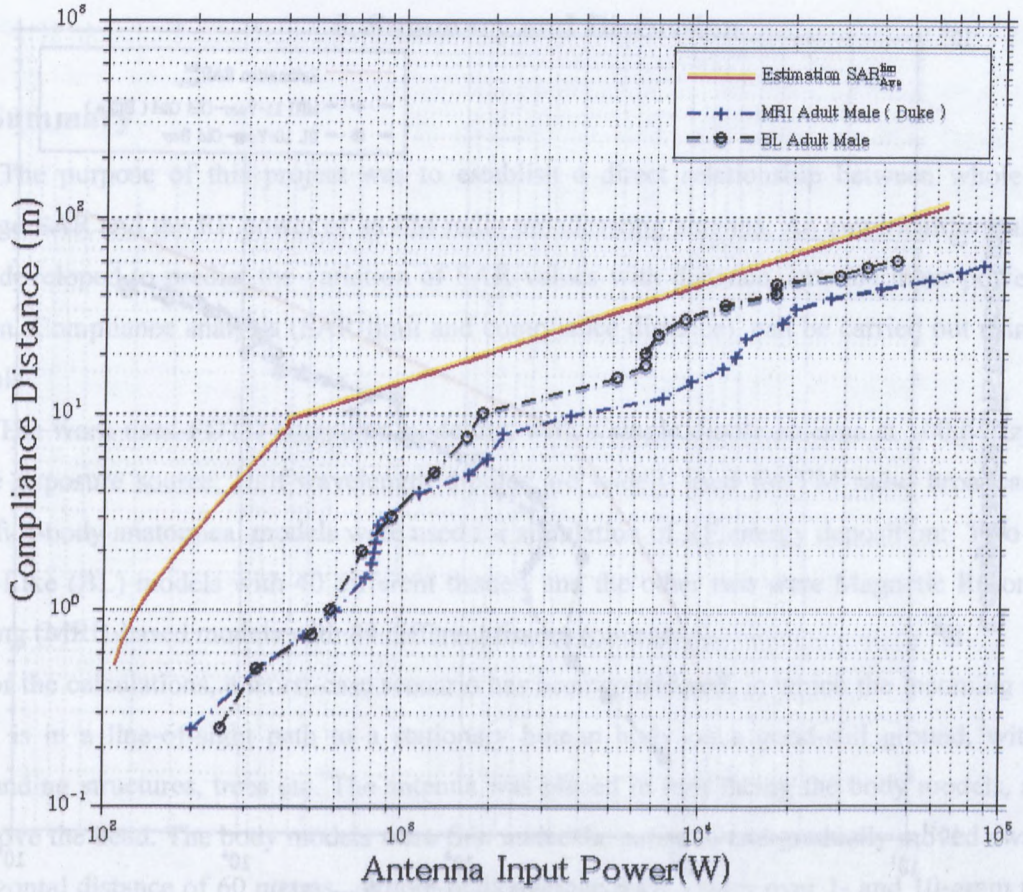

Figure 4.4 Compliance Distances for Adult Models Versus Antenna Input Power. Solid red line is the estimated value. The simulation data for the two male adult bodies are displayed for comparison.

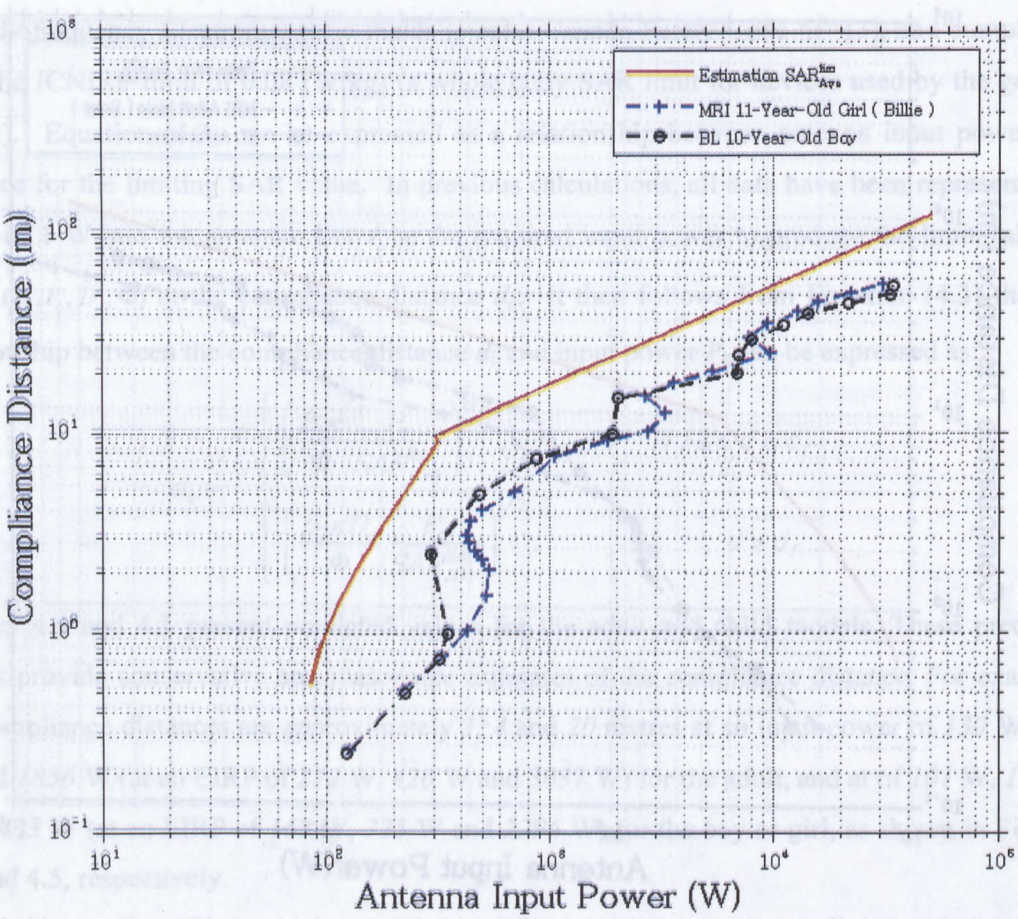

Figure 4.5 Compliance Distances for Child Models Versus Antenna Input Power. Solid red line is the estimated value. The simulation data for the two child models are displayed for comparison.

5. Summary and Discussion

5.1 Summary

The purpose of this project was to establish a direct relationship between whole-body average SAR and the RF power of an FM radio broadcasting antenna. An empirical formula has been developed to predict the variation of SAR values with distance, antenna input power and pattern. Compliance analysis (SAR limit and compliance distance), can be carried out using the formula.

The work used FDTD computer modeling, with a single dipole antenna at 100 MHz used as the exposure source. Half-wavelength dipoles are widely used for FM radio broadcasting. Four full-body anatomical models were used for simulation of RF energy deposition: Two were Body-Like (BL) models with 40 different tissues, and the other two were Magnetic Resonance Imaging (MRI)-based models with 84 different tissues (or organs).

For the calculations, a worst-case scenario has been considered, in which the incoming radio signal is in a line-of-sight path to a stationary human body on a good-soil ground, with no surrounding structures, trees etc. The antenna was placed in turn facing the body models, at 15 cm above the head. The body models were first under the antenna, and gradually moved away to a horizontal distance of 60 metres. Whole-body average SAR values over 1- and 10-gram mass have been calculated according to IEEE Std. C95.3-2002 (R2008). With the maxima location feature and voxel editor of the Empire FDTD program, peak spatial-averaged SAR values and their tissue locations were obtained.

Variation of whole-body average SAR with distance exhibits a characteristic behaviour: in that the whole-body average SAR decays with distance as $1/r^{\delta}$ ($\delta \approx 0.6$) in the near-field region, and approximately as $1/r^2$ in the far-field region. Two piecewise approximate expressions were obtained by a linear fit with a logarithmic scale coordinate system, expressed as a function of distance by using a path slope in each region.

5.2 Main Results

Based on the numerical results, two estimation formulas were developed to describe whole-body average SAR. Equation (4.3) estimates the variation of whole-body average SAR with distance, Figure 5.1, and Equation (4.6) predicts the compliance distance as a function of input

power, Figure 5.2. Both formulas are reasonably conservative in nature, and easy to use for practical assessment purposes. The formulas can be used for all antennas with electrical dimensional size not larger than four wavelengths [18]. The body size effect on SAR is approximately the inverse of the body average thickness. In the current study, an 11-year-old girl and a 10-year-old boy have been considered, also shown in Figures 5.1 and 5.2. Further work could consider other size body models, such as different age children and women.

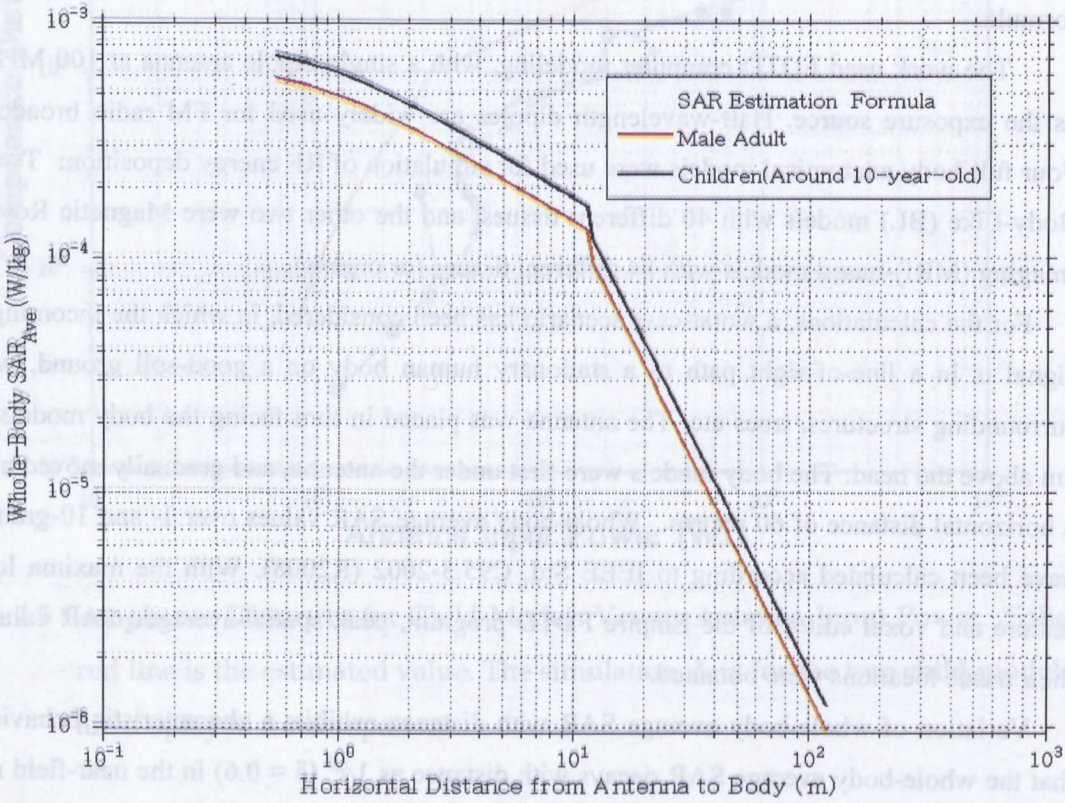

Figure 5.1 Estimation Formula for Whole-Body Average SAR Values with Distance.

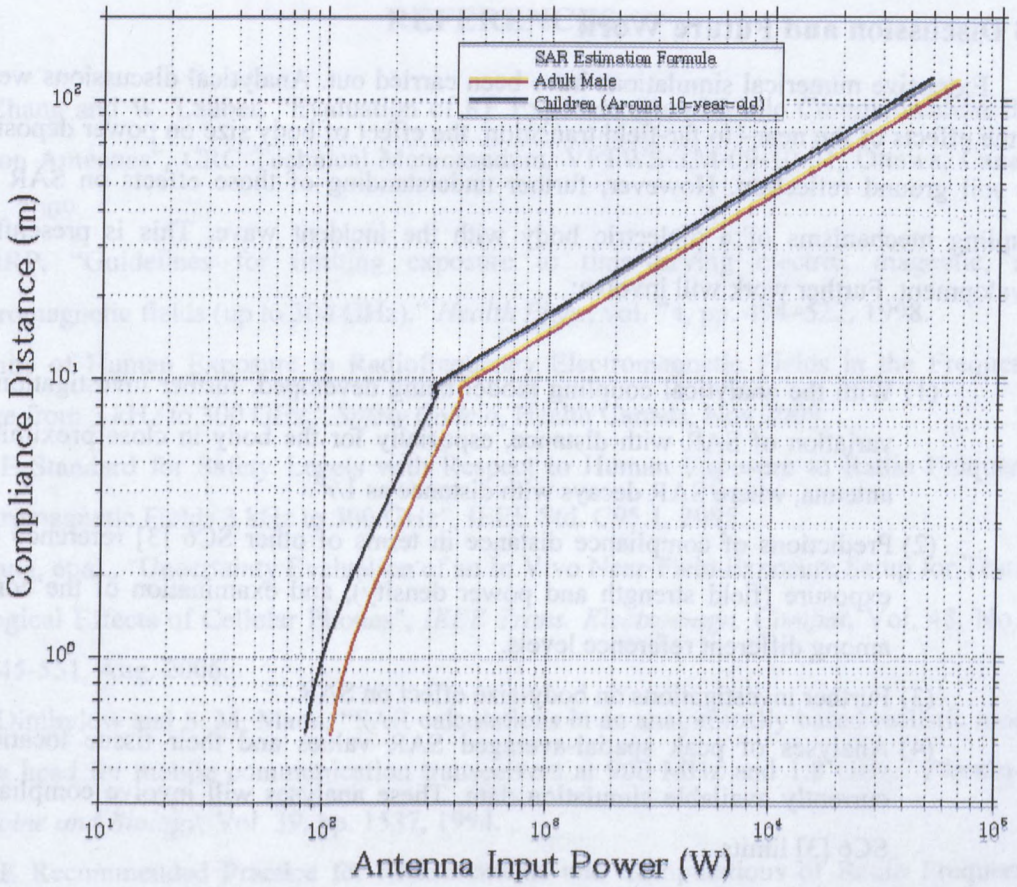

Figure 5.2 Estimation Formula for Compliance Distance as a Function of Antenna Input Power.

5.3 Discussion and Future Work

Extensive numerical simulations have been carried out. Analytical discussions were given on the effects of the near– to far-field transition, the effect of body size on power deposition and the soil ground reflection. However, further understanding of those effects on SAR requires coupling mechanisms of a dielectric body with the incident wave. This is presently under development. Further work will involve:

(1) With the analytical coupling model being developed, further investigations on the variation of SAR with distance, especially for the body in close proximity to the antenna, where SAR decays with distance as $1/r^{\delta}$.

(2) Predictions of compliance distance in terms of other SC6 [3] reference levels of exposure (field strength and power density), and examination of the consistency among different reference levels.

(3) Further investigations on body-size effect on SAR.

(4) Analyses of peak spatial-averaged SAR values and their tissue locations with currently available simulation data. These analyses will involve compliance with SC6 [3] limits.

REFERENCES

[1] M. Zhang and W. Lauber, "Evaluation of RF Exposure from Mobile Communication Base Station Antennas", CRC Technical Memorandum, VPTWS-TM-09-10-01, Ottawa, Canada, Nov., 2009.

[2]ICNIRP, "Guidelines for limiting exposure to time-varying electric, magnetic, and electromagnetic fields (up to 300 GHz)," *Health Phys.*, vol. 74, pp. 494–522, 1998.

[3] "Limits of Human Exposure to Radiofrequency Electromagnetic Fields in the Frequency Range from 3 kHz to 300 GHz," *Safety Code 6*, Health Canada, Nov.2009.

[4] "IEEE Standard for Safety Levels with Respect to Human Exposure to Radio Frequency Electromagnetic Fields 3 kHz to 300 GHz", IEEE Std. C95.1, 2005.

[5] J. Wang, et al., "Uncertainty Evaluation of an In Vivo Near-Field Exposure Setup for Testing Biological Effects of Cellular Phones", *IEEE Trans. Electromagn. Compat*, Vol. 48, No. 3, pp. 545-551, Aug. 2006.

[6] P. J. Dimbylow and S. M. Mann, "SAR calculations in an anatomically based realistic model of the head for mobile communication transceivers at 900 MHz and 1.8 GHz." *Physics in Medicine and Biology,* Vol. 39, pp. 1537, 1994.

[7] "IEEE Recommended Practice for Measurements and Computations of Radio Frequency Electromagnetic Fields with Respect to Human Exposure to such Fields, 3 kHz to 300 GHz", IEEE Std. C95.3-2002 (R2008).

[8] User's Manual for EMPIRE, version 5.30, Nov. 2008, at: http://www.empire.de/.

[9] High-Resolution Whole-Body Human Models provided by ITIS Foundation at: http://www.itis.ethz.ch/index/index_humanmodels.html.

[10] Tissue Dielectric Parameters provided by Italian National Council webpage at: http://niremf.ifac.cnr.it/tissprop/htmlclie/htmlclie.htm#stsftag.

[11] Tissue Dielectric Parameters provided by FCC webpage at: http://www.fcc.gov/oet/rfsafety/dielectric.html.

[12] L. Sandrini, et al., "RF dosimetry: a comparison between power absorption of female and male numerical models from 0.1 to 4 GHz," *Physics in Medicine and Biology,* Vol. 49, pp. 5185-5201, 2004.

[13] Electroherbalism, "Electrical and Frequency Effects on Pathogens," at: http://www.electroherbalism.com/Bioelectronics/IntroductiontoBioelectronics/ElectricalandFrequencyEffectsonPathogens.htm.

or:

J. M. RANDALL, et al., "Resonant frequencies of standing humans," *Ergonomics*, Vol. 40, pp. 879 – 886, Sept. 1997.

[14] J. Wang, et al., "FDTD calculation of whole-body average SAR in adult and child models for frequencies from 30 MHz to 2GHz." *Physics in Medicine and Biology,* Vol. 51, pp. 4119-4127, 2006.

[15] National Council on Radiation Protection and Measurements, a Practical Guide to the Determination of Human Exposure to Radiofrequency Fields. NCRP Report No.119: Bethseda, MD, 1993.

[16] A. Dorne, Chapter 4, 'Cone and cylinder antennas' in Radio Research Laboratory Harvard University, *Very High-Frequency Techniques, Volume I.* New York and London: McGraw-Hill Book Company, Inc., 1947.

[17] R. Cicchetti and A. Faraone, "Estimation of the peak power density in the vicinity of cellular and radio base station antennas," *IEEE Trans. Electromagn. Compat.*, vol. 46, no. 2, pp. 275–290, May 2004.

[18] B. Thors, et al., "On the Estimation of SAR and Compliance Distance Related to RF Exposure from Mobile Communication Base Station Antennas ," *IEEE Trans. Electromagn. Compat.*, vol. 50, no. 4, pp. 837–848, Nov. 2008.